Isoperimetric Conjugate Points with Application to the Stability of DNA Minicircles

Robert S. Manning[1], Kathleen A. Rogers[2], and John H. Maddocks[3]

Institute for Physical Science and Technology
and Department of Mathematics
University of Maryland
College Park, MD 20742

http://www.lcvm.umd.edu/
rmanning@masg1.epfl.ch, krogers@ima.umn.edu,
maddocks@dma.epfl.ch

March 24, 2005

[1]Current Address: Département de Mathématiques; Ecole Polytechnique Fédérale de Lausanne; CH-1015 Lausanne Switzerland

[2]Current Address: Institute for Mathematics and its Applications; 206 Church Street SE; Minneapolis, MN 55455-0436 USA

[3]Author to whom correspondence should be addressed, Current Address: Département de Mathématiques; Ecole Polytechnique Fédérale de Lausanne; CH-1015 Lausanne Switzerland

Abstract

A conjugate point test determining an index of the constrained second variation in one-dimensional isoperimetric calculus of variations problems is described. The test is then implemented numerically to determine stability properties of equilibria within a continuum mechanics model of DNA minicircles.

Keywords: elastic rods, bifurcation diagrams, two-point boundary conditions, constrained second variation, index

1 Introduction

Recently there has been considerable interest in using elastic rod theories in the simulation of DNA (cf. the extensive survey articles by Schlick [26] and Olson [20]). In Manning et al. [18], the formulation of elastic rods presented in Li and Maddocks [16] was used to approximate the equilibrium configurations of DNA minicircles as critical points of a one-dimensional calculus of variations problem involving isoperimetric constraints. (Minicircles are DNA molecules of approximately 150 base-pairs that have been cyclized; i.e. the double helix forms a covalently closed ring.) In this article, we derive a constrained conjugate point test which assigns an isoperimetric index to each constrained critical point, and apply it to the DNA minicircle example. The isoperimetric index gives the maximal dimension of a space on which the second variation can be made negative, and thus, for example, is a valuable tool for identifying those critical points that are actually local minima of the potential, since local minima must have non-negative second variation and isoperimetric index zero.

For unconstrained calculus of variations problems, the absence of a conjugate point on an extremal (Jacobi's condition) is a well-known necessary condition for the extremal to be an unconstrained local minimum (cf. [9, p. 112], for example). Morse [19] later introduced the notion of *counting* conjugate points of the second variation operator to determine an index. For the isoperimetric problem, Bolza (see [4, p. 220] and references therein) derived a test for a constrained local minimum based on the absence of an isoperimetric conjugate point. In this paper, we set forth an alternate derivation of isoperimetric conjugate points, and, analogous to the extension by Morse in the unconstrained case, use our approach to demonstrate that an isoperimetric index can be defined by counting conjugate points for an appropriately projected second variation operator. Our formulation also leads naturally to an efficient numerical algorithm for determination of isoperimetric conjugate points, and hence the isoperimetric index, for families of extremals. This algorithm involves the computation of the determinant of a constrained stability matrix whose entries are solutions to appropriate initial value problems.

In the DNA minicircle example, the variational principle involves minimization of a potential energy, so it is natural to define a stable equilibrium to be one that has isoperimetric index zero. Applying the isoperimetric index calculation to the DNA example reveals the presence of at least two stable minicircle configurations for each of the eleven molecules studied in [18], which was an unanticipated conclusion (see Sec. 5 for a description of a typical molecule). In addition, the dependence of stability on an important physical parameter (the ratio of twisting to bending stiffness) is investigated, and interesting behavior uncovered.

Sec. 2.1 contains a derivation of the standard unconstrained conjugate point test from a particular perspective that is amenable to the extension to the isoperimetrically constrained case that is described in Sec. 2.2. In Sec. 3, we define a constrained stability matrix used to determine isoperimetric conjugate points, and describe the determination of this matrix via numerical solution of initial value problems. Our twisted elastic rod model for DNA minicircles is introduced in Sec. 4, including the specific form of the required second variation. Sec. 5 contains the results of the stability computations in the DNA example. Finally, Sec. 6 contains a discussion of our results, as well as a comparison between the isoperimetric conjugate point test developed here and stability exchange predictions arising from bifurcation theory.

2 Conjugate Points and Indices

2.1 The Unconstrained Case

In this subsection, we set notation and present a self-contained treatment of the standard conjugate point theory in unconstrained calculus of variations problems from a perspective that makes an extension to isoperimetrically constrained problems most transparent. We consider a functional of the form:[4]

$$\begin{aligned} J[\mathbf{q}] &= \int_0^1 L(\mathbf{q}, \mathbf{q}', s)\, ds, \quad \mathbf{q}(s) \in \mathbb{R}^p, \\ &\text{subject to } \ \mathbf{q}(0) = \mathbf{h}_0, \ \ \mathbf{q}(1) = \mathbf{h}_1. \end{aligned} \tag{1}$$

Most of the results cited in this subsection are an established part of the classic unconstrained calculus of variations literature and can be found in many standard texts, e.g. [8, 9, 12, 25]. However, index (or signature) theory appears only in more modern treatments [10, 19].

Critical points $\mathbf{q}_0(s)$ are solutions to the standard Euler-Lagrange equations for the functional J. Classification of these critical points involves an analysis of the second variation of (1) at $\mathbf{q}_0$, namely

$$\delta^2 J[\boldsymbol{\zeta}] = \frac{1}{2} \int_0^1 \left[(\boldsymbol{\zeta}')^T \mathbf{P} \boldsymbol{\zeta}' + (\boldsymbol{\zeta}')^T \mathbf{C}^T \boldsymbol{\zeta} + \boldsymbol{\zeta}^T \mathbf{C} \boldsymbol{\zeta}' + \boldsymbol{\zeta}^T \mathbf{Q} \boldsymbol{\zeta} \right] \, ds, \tag{2}$$

where $\mathbf{P} = L_{\mathbf{q}'\mathbf{q}'}$, $\mathbf{C} = L_{\mathbf{q}\mathbf{q}'}$, and $\mathbf{Q} = L_{\mathbf{q}\mathbf{q}}$ are all s-dependent $p \times p$ matrices evaluated at $\mathbf{q}_0(s)$. We assume throughout that Legendre's strengthened condition holds

$$\mathbf{P} > 0, \tag{3}$$

[4] We only consider Dirichlet boundary conditions; conjugate point tests exist for more general boundary conditions, but they can be more complicated.

i.e. the symmetric matrix $\mathbf{P}$ is positive definite. Here $\boldsymbol{\zeta}$ is a variation in the solution that, due to the boundary conditions on $\mathbf{q}_0$, must lie in the set of admissible variations:

$$\mathcal{A}_d \equiv \{\boldsymbol{\zeta} : \boldsymbol{\zeta}(0) = \mathbf{0} = \boldsymbol{\zeta}(1)\}\,.$$

With these boundary conditions, an alternate form of the second variation is achieved after an integration by parts:

$$\delta^2 J[\boldsymbol{\zeta}] \;\; = \;\; \frac{1}{2}\int_0^1 \boldsymbol{\zeta}^T\,(\mathcal{S}\boldsymbol{\zeta})\;\, ds,$$

where $\mathcal{S}$ is the self-adjoint second-order vector differential operator:

$$\mathcal{S}\boldsymbol{\zeta} \equiv -\frac{d}{ds}\left[\mathbf{P}\boldsymbol{\zeta}' + \mathbf{C}^T\boldsymbol{\zeta}\right] + \mathbf{C}\boldsymbol{\zeta}' + \mathbf{Q}\boldsymbol{\zeta}. \tag{4}$$

(Standard issues concerning domains of definition of quadratic forms of the type (2) and densely defined differential operators of the form (4) arise (see, for example, [21] §VIII.6), but are not of primary concern here.)

A necessary condition for $\mathbf{q}_0$ to be a local minimum of J is that

$$\delta^2 J[\boldsymbol{\zeta}] \geq 0, \;\; \forall \boldsymbol{\zeta} \in \mathcal{A}_d. \tag{5}$$

Given Legendre's strengthened condition (3), condition (5) is equivalent to Jacobi's necessary condition, namely that $\mathbf{q}_0$ has no *conjugate point*, where a conjugate point is defined to be a value $\sigma < 1$ for which there is a nontrivial solution to:

$$\mathcal{S}\boldsymbol{\zeta} = \mathbf{0}, \;\; 0 < s < \sigma, \;\; \boldsymbol{\zeta}(0) = \boldsymbol{\zeta}(\sigma) = \mathbf{0}.$$

Morse [19] extended Jacobi's condition to use the *number* of conjugate points to define an index which quantifies the dimension of the set on which $\delta^2 J$ is negative; our presentation of the index is not the one taken by Morse, but rather an equivalent form suitable for extension to the constrained case. We embed Jacobi's condition into the eigenvalue problem

$$\mathcal{S}\boldsymbol{\zeta} = \rho\boldsymbol{\zeta}, \;\; 0 < s < \sigma \leq 1, \;\; \boldsymbol{\zeta}(0) = \boldsymbol{\zeta}(\sigma) = \mathbf{0}. \tag{6}$$

The eigenvalues ρ will generally depend on σ, so we denote them $\rho(\sigma)$. Conjugate points are then values of σ for which (6) has $\rho(\sigma) = 0$ as an eigenvalue. Using Legendre's strengthened condition, Rayleigh quotients, and other techniques (see e.g., the proofs in Appendix A for the constrained case), one can derive the following three properties:

Property 1: For prescribed σ, the spectrum of $\mathcal{S}$ consists of isolated eigenvalues $\rho_1(\sigma) \leq \rho_2(\sigma) \leq \cdots$, each with finite multiplicity,
Property 2: Each eigenvalue $\rho_j(\sigma)$ is a monotonically decreasing function of σ, and

Property 3: For σ sufficiently close to 0, $\rho_j(\sigma) > 0$ for all j.

The *index* I of the extremal $\mathbf{q}_0$ is then defined to be the number of eigenvalues $\rho_j(1)$ of (6) which are negative. Due to Properties 1–3, the index is equal to the number of conjugate points $\sigma < 1$, counted according to multiplicity.[5] If $I = 0$, then Jacobi's necessary condition holds, and we shall describe $\mathbf{q}_0$ as *stable*. If $I > 0$, then $\mathbf{q}_0$ is not a local minimum (in any of the standard topologies), and in fact there is a subspace of variations of dimension I on which $\delta^2 J < 0$.

2.2 The Isoperimetric Case

The focus of this paper is to extend the notion of index to isoperimetrically constrained calculus of variations problems involving functionals of the form:[6]

$$\begin{aligned} W[\mathbf{q}] &= \int_0^1 L(\mathbf{q}, \mathbf{q}', s)\, ds, \quad \mathbf{q}(s) \in \mathbb{R}^p, \\ \text{subject to} \quad & \int_0^1 g_i(\mathbf{q})\, ds = 0, \quad i = 1, \dots n, \\ & \mathbf{q}(0) = \mathbf{h}_0, \quad \mathbf{q}(1) = \mathbf{h}_1. \end{aligned} \tag{7}$$

According to the usual multiplier rule, an associated functional

$$J[\mathbf{q}] = \int_0^1 \left(L + \mathbf{g}^T \boldsymbol{\lambda}\right)\, ds$$

is constructed, and constrained critical points $(\mathbf{q}_0(s), \boldsymbol{\lambda}_0)$ of W are solutions of the standard unconstrained Euler-Lagrange equations for the functional J, with the multiplier $\boldsymbol{\lambda}_0$ determined by the integral constraints. The second variation $\delta^2 J$, and its associated operator $\mathcal{S}$, take the unconstrained forms (2) and (4), but now with $\mathbf{Q} = \mathbf{g}^T_{\mathbf{qq}} \boldsymbol{\lambda}_0 + L_{\mathbf{qq}}$. Admissible variations $\boldsymbol{\zeta}$ must satisfy the linearized constraints

$$\int_0^1 \boldsymbol{\zeta}^T \frac{\partial g_i}{\partial \mathbf{q}}(\mathbf{q}_0)\, ds = 0,$$

giving rise to the admissible set of constrained variations:

$$\mathcal{A}_d^{cons} \equiv \left\{ \boldsymbol{\zeta} \in \mathcal{A}_d : \int_0^1 \boldsymbol{\zeta}^T \mathbf{T}_i\, ds = 0, \quad i = 1, \cdots, n \right\},$$

[5] This conclusion relies on both the isolation of the conjugate points σ and on the continuity of $\rho_j(\sigma)$ with respect to σ. Theorems guaranteeing these properties are available in the unconstrained setting; for example, isolation of conjugate points has been proven by Morse [19] and the continuity of ρ is discussed, e.g., in Kato [14].

[6] For notational convenience, we only consider isoperimetric constraints with integrands of the form $g_i(\mathbf{q}(s))$, although the analysis can immediately be extended to the more general case $g_i(\mathbf{q}(s), \mathbf{q}'(s), s)$.

where:

$$\mathbf{T}_i \equiv \frac{\partial g_i}{\partial \mathbf{q}}(\mathbf{q}_0).$$

We assume that the $\mathbf{T}_i(s)$ are linearly independent (as functions of s) on every interval $(0, \sigma)$ for $0 < \sigma < 1$.

A necessary condition for $\mathbf{q}_0$ to realize a constrained local minimum is (cf. [12, p. 85])

$$\delta^2 J[\boldsymbol{\zeta}] \geq 0, \quad \forall \boldsymbol{\zeta} \in \mathcal{A}_d^{cons}. \tag{8}$$

Bolza [4] used a completion of squares argument (in the case $(p, n) = (2, 1)$ and citing work of Weierstrass and Kneser), to show that condition (8) is equivalent to an extremal having no *isoperimetric conjugate point*, where $\sigma < 1$ is called an isoperimetric conjugate point if the following system has a nontrivial solution:

$$\begin{aligned} &\mathcal{S}\boldsymbol{\zeta} = \sum_{i=1}^{n} \breve{c}_i \mathbf{T}_i, \quad 0 < s < \sigma, \quad \text{for some constants } \breve{c}_i, \\ &\boldsymbol{\zeta}(0) = \boldsymbol{\zeta}(\sigma) = \mathbf{0}, \qquad \int_0^\sigma \boldsymbol{\zeta}^T \mathbf{T}_i \, ds = 0, \quad i = 1, \ldots, n. \end{aligned} \tag{9}$$

Bolza also presented this condition in the equivalent form (15) presented in Sec. 3.

In this paper we modify this notion of isoperimetric conjugate point to allow an isoperimetric index to be defined as the number of isoperimetric conjugate points. To this end, we introduce an eigenvalue problem analogous to (6) that admits a Rayleigh quotient. We proceed via the introduction of an orthogonal projection operator, denoted by $\mathcal{Q}$ (see Eq. (33) in Appendix A), onto the L^2-orthogonal complement of $\mathcal{T} \equiv \text{span}(\mathbf{T}_1, \ldots, \mathbf{T}_n)$. In Lemma 1 of Appendix A, we show that the condition

$$\begin{aligned} &\mathcal{Q}\mathcal{S}\mathcal{Q}\boldsymbol{\zeta} = \mathbf{0}, \quad 0 < s < \sigma, \quad \boldsymbol{\zeta} \not\equiv \mathbf{0}, \\ &\boldsymbol{\zeta}(0) = \boldsymbol{\zeta}(\sigma) = \mathbf{0}, \qquad \int_0^\sigma \boldsymbol{\zeta}^T \mathbf{T}_i \, ds = 0, \quad i = 1, \ldots, n \end{aligned} \tag{10}$$

is equivalent to Bolza's definition of an isoperimetric conjugate point (9). In addition, as shown in Appendix A, if we consider an eigenvalue problem analogous to (6):

$$\begin{aligned} &\mathcal{Q}\mathcal{S}\mathcal{Q}\boldsymbol{\zeta} = \rho(\sigma)\boldsymbol{\zeta}, \quad 0 < s < \sigma, \quad \boldsymbol{\zeta} \not\equiv \mathbf{0}, \\ &\boldsymbol{\zeta}(0) = \boldsymbol{\zeta}(\sigma) = \mathbf{0}, \qquad \int_0^\sigma \boldsymbol{\zeta}^T \mathbf{T}_i \, ds = 0, \quad i = 1, \ldots, n, \end{aligned} \tag{11}$$

we may again prove Properties 1–3 from Sec. 2.1, now for the projected operator $\mathcal{Q}\mathcal{S}\mathcal{Q}$. We then define the *isoperimetric index* I to be the number of eigenvalues $\rho_j(1)$ that are negative. As shown in Lemma 2 of Appendix

A, if $I = 0$ then the necessary condition (8) holds, and we describe $\mathbf{q}_0$ as stable, while if $I > 0$, then $\mathbf{q}_0$ is not a constrained local minimum, and in fact there is a subspace of constrained variations of dimension I on which $\delta^2 J < 0$.

As in the unconstrained setting, we can conclude from Properties 1–3 that the isoperimetric index can be computed as the number of isoperimetric conjugate points $\sigma < 1$, subject to the assumptions of isolation of conjugate points and continuity of $\rho_j(\sigma)$ with respect to σ. In contrast to the unconstrained setting, we are not aware of any general theorems immediately guaranteeing that the assumptions of continuity and isolation hold. In particular, the presence of an integral operator in the eigenvalue problem (11) prevents the transparent extension of the unconstrained theory to the isoperimetric case. However, in practice, the failure of either of these assumptions would be apparent in numerical implementation and did not occur in the examples we studied. In the event that these assumptions do not hold, the index still provides a lower bound for the dimension of set of variations on which $\delta^2 J < 0$, so that $\mathbf{q}_0$ having index zero is still a necessary condition for $\mathbf{q}_0$ to be a constrained local minimum.

3 Numerical Implementation

As is well known, unconstrained conjugate points can be computed as roots of an appropriate $p \times p$, s-dependent determinant [25]. In this section, we present an analogous test for isoperimetric conjugate points involving a determinant of an augmented $(p+n) \times (p+n)$ matrix.

3.1 The Constrained Stability Matrix

The goal of this section is to construct a finite-dimensional system of linear algebraic equations that is equivalent to the definition of isoperimetric conjugate point (9). We first find a general solution to the homogeneous initial value problem:

$$\mathcal{S}\boldsymbol{\zeta} = \mathbf{0}, \quad \boldsymbol{\zeta}(0) = \mathbf{0},$$

which includes p undetermined constants:

$$\boldsymbol{\zeta} = c_1\boldsymbol{\zeta}_1 + c_2\boldsymbol{\zeta}_2 + \cdots + c_p\boldsymbol{\zeta}_p.$$

Similarly, for each $\mathbf{T}_i$, we find a single solution to the initial value problem

$$\mathcal{S}\breve{\boldsymbol{\zeta}}_i = \mathbf{T}_i, \quad \breve{\boldsymbol{\zeta}}_i(0) = \mathbf{0}.$$

Then, the function

$$\boldsymbol{\zeta} = \sum_{i=1}^{p} c_i\boldsymbol{\zeta}_i + \sum_{i=1}^{n} \breve{c}_i\breve{\boldsymbol{\zeta}}_i$$

is the general solution to

$$\mathcal{S}\boldsymbol{\zeta} = \sum_{i=1}^{n} \breve{c}_i \mathbf{T}_i, \quad \boldsymbol{\zeta}(0) = \mathbf{0}.$$

The system (9) will have a solution if and only if there exist constants c_i and $\breve{c}_i$ such that $\boldsymbol{\zeta}(s)$ satisfies the boundary conditions at $s = \sigma$

$$\sum_{j=1}^{p} c_j \boldsymbol{\zeta}_j(\sigma) + \sum_{j=1}^{n} \breve{c}_j \breve{\boldsymbol{\zeta}}_j(\sigma) = \mathbf{0}, \tag{12}$$

and the (linearized) constraints

$$\int_0^\sigma \left[\sum_{j=1}^{p} c_j \boldsymbol{\zeta}_j(\tau) + \sum_{j=1}^{n} \breve{c}_j \breve{\boldsymbol{\zeta}}_j(\tau) \right]^T \mathbf{T}_i(\tau)\, d\tau = 0, \;\; i = 1, \ldots, n. \tag{13}$$

Eqs. (12) and (13) can be written in matrix form:

$$\mathbf{M}(\sigma) \begin{bmatrix} \mathbf{c} \\ \breve{\mathbf{c}} \end{bmatrix} \equiv \begin{bmatrix} \mathbf{A}(\sigma) & \breve{\mathbf{A}}(\sigma) \\ \mathbf{F}(\sigma) & \breve{\mathbf{F}}(\sigma) \end{bmatrix} \begin{bmatrix} \mathbf{c} \\ \breve{\mathbf{c}} \end{bmatrix} = \mathbf{0}, \tag{14}$$

where

$$\begin{aligned}
\mathbf{c} &= [c_1 \ldots c_p]^T \in \mathbb{R}^p, \\
\breve{\mathbf{c}} &= [\breve{c}_1 \ldots \breve{c}_n]^T \in \mathbb{R}^n, \\
\mathbf{A}(\sigma) &= \begin{bmatrix} \boldsymbol{\zeta}_1(\sigma) & \ldots & \boldsymbol{\zeta}_p(\sigma) \end{bmatrix} \in \mathbb{R}^{p \times p}, \\
\breve{\mathbf{A}}(\sigma) &= \begin{bmatrix} \breve{\boldsymbol{\zeta}}_1(\sigma) & \ldots & \breve{\boldsymbol{\zeta}}_n(\sigma) \end{bmatrix} \in \mathbb{R}^{p \times n}, \\
\mathbf{F}(\sigma) &= \{f_{ij}(\sigma)\} = \left\{ \int_0^\sigma \boldsymbol{\zeta}_j(\tau)^T \mathbf{T}_i(\tau) d\tau \right\} \in \mathbb{R}^{n \times p}, \\
\breve{\mathbf{F}}(\sigma) &= \left\{ \breve{f}_{ij}(\sigma) \right\} = \left\{ \int_0^\sigma \breve{\boldsymbol{\zeta}}_j(\tau)^T \mathbf{T}_i(\tau) d\tau \right\} \in \mathbb{R}^{n \times n}.
\end{aligned}$$

Eq. (14), and therefore Eq. (9), has a nontrivial solution only at values of σ for which the $(p+n) \times (p+n)$ *constrained stability matrix* $\mathbf{M}(\sigma)$ satisfies

$$\det \mathbf{M}(\sigma) = 0. \tag{15}$$

These σ values are precisely the isoperimetric conjugate points. An analogous test for unconstrained conjugate points is obtained by setting $n = 0$ to arrive at $\det \mathbf{A}(\sigma) = 0$ ([25], p. 152).

In summary, Eqs. (9), (10), and (15) are all equivalent definitions of isoperimetric conjugate points. Of the three, Eq. (10) is a particularly suitable form for analysis, e.g. the results proven in Appendix A. In contrast, Eq. (15) is the most suitable form for computation, as further described in the remainder of this section.

3.2 Computing homogeneous and nonhomogeneous solutions

As shown in Sec. 3.1, construction of the matrix $\mathbf{M}$ requires the computation of a basis of p solutions $\boldsymbol{\zeta}_1, \ldots, \boldsymbol{\zeta}_p$ of the homogeneous equation

$$-\frac{d}{ds}\left[\mathbf{P}\boldsymbol{\zeta}' + \mathbf{C}^T\boldsymbol{\zeta}\right] + \mathbf{C}\boldsymbol{\zeta}' + \mathbf{Q}\boldsymbol{\zeta} = \mathbf{0}, \quad \boldsymbol{\zeta}(0) = \mathbf{0}, \tag{16}$$

and one solution $\breve{\boldsymbol{\zeta}}_i$ for each of the n non-homogeneous equations

$$-\frac{d}{ds}\left[\mathbf{P}\boldsymbol{\zeta}' + \mathbf{C}^T\boldsymbol{\zeta}\right] + \mathbf{C}\boldsymbol{\zeta}' + \mathbf{Q}\boldsymbol{\zeta} = \mathbf{T}_i, \quad \boldsymbol{\zeta}(0) = \mathbf{0}. \tag{17}$$

These solutions can be numerically computed from appropriate initial value problems (IVPs), as outlined here. We first rewrite the second-order differential equations (16) and (17) as first-order systems, by defining

$$\mathbf{v} \equiv \mathbf{P}\boldsymbol{\zeta}' + \mathbf{C}^T\boldsymbol{\zeta}.$$

Solving for $\boldsymbol{\zeta}'$ in terms of $\mathbf{v}$ and $\boldsymbol{\zeta}$ leads to the first-order systems:

$$\begin{aligned} \boldsymbol{\zeta}' &= \mathbf{P}^{-1}(\mathbf{v} - \mathbf{C}^T\boldsymbol{\zeta}), \\ \mathbf{v}' &= \mathbf{C}\boldsymbol{\zeta}' + \mathbf{Q}\boldsymbol{\zeta} \qquad = \mathbf{C}\mathbf{P}^{-1}(\mathbf{v} - \mathbf{C}^T\boldsymbol{\zeta}) + \mathbf{Q}\boldsymbol{\zeta}, \\ \boldsymbol{\zeta}(0) &= \mathbf{0}, \end{aligned}$$

and

$$\begin{aligned} \breve{\boldsymbol{\zeta}}' &= \mathbf{P}^{-1}(\breve{\mathbf{v}} - \mathbf{C}^T\breve{\boldsymbol{\zeta}}), \\ \breve{\mathbf{v}}' &= \mathbf{C}\breve{\boldsymbol{\zeta}}' + \mathbf{Q}\breve{\boldsymbol{\zeta}} - \mathbf{T}_i = \mathbf{C}\mathbf{P}^{-1}(\breve{\mathbf{v}} - \mathbf{C}^T\breve{\boldsymbol{\zeta}}) + \mathbf{Q}\breve{\boldsymbol{\zeta}} - \mathbf{T}_i, \\ \breve{\boldsymbol{\zeta}}(0) &= \mathbf{0}. \end{aligned}$$

Finally, we need to specify the appropriate initial conditions for $\mathbf{v}$. For the homogeneous case, a basis of solutions to (16) is provided by using p linearly independent initial values for $\mathbf{v}(0)$, e.g.

$$\mathbf{v}_i(0) = \mathbf{e}_i, \quad i = 1, \ldots, p.$$

For the nonhomogeneous solutions, any initial conditions on $\breve{\mathbf{v}}$ will suffice, and we use $\breve{\mathbf{v}}(0) = \mathbf{0}$. The resulting $\breve{\boldsymbol{\zeta}}_i$ will be linearly independent, since we have assumed that the $\mathbf{T}_i(s)$ are linearly independent on all intervals $(0, \sigma)$.

3.3 Computing the integrals in the constrained stability matrix

The sub-blocks $\mathbf{F}$ and $\breve{\mathbf{F}}$ of the matrix $\mathbf{M}$ consist of the integrals $f_{ij}(\sigma) \equiv \int_0^\sigma \boldsymbol{\zeta}_j(\tau)^T \mathbf{T}_i(\tau) d\tau$ and $\breve{f}_{ij}(\sigma) \equiv \int_0^\sigma \breve{\boldsymbol{\zeta}}_j(\tau)^T \mathbf{T}_i(\tau) d\tau$, which also can be computed by solving an IVP. Assuming that the functions $\boldsymbol{\zeta}_j(\sigma)$ and $\breve{\boldsymbol{\zeta}}_j(\sigma)$ have been computed (as described in Sec. 3.2), the differential equations for f_{ij} and $\breve{f}_{ij}$ are:

$$
\begin{aligned}
f'_{ij}(\sigma) &= \boldsymbol{\zeta}_j(\sigma)^T \mathbf{T}_i(\sigma), \\
\breve{f}'_{ij}(\sigma) &= \breve{\boldsymbol{\zeta}}_j(\sigma)^T \mathbf{T}_i(\sigma),
\end{aligned}
$$

with $f_{ij}(0) = \breve{f}_{ij}(0) = 0$.

3.4 Assembling the IVP

In summary, to determine conjugate points, we solve the following system of $(n+p)(n+2p)$ first-order differential equations:

$$
\begin{aligned}
\boldsymbol{\zeta}_i{}' &= \mathbf{P}^{-1}(\mathbf{q}_0)(\mathbf{v}_i - \mathbf{C}^T(\mathbf{q}_0)\boldsymbol{\zeta}_i), \\
\mathbf{v}_i{}' &= \mathbf{C}(\mathbf{q}_0)\mathbf{P}^{-1}(\mathbf{q}_0)(\mathbf{v}_i - \mathbf{C}^T(\mathbf{q}_0)\boldsymbol{\zeta}_i) + \mathbf{Q}(\mathbf{q}_0)\boldsymbol{\zeta}_i, \\
\breve{\boldsymbol{\zeta}}'_i &= \mathbf{P}^{-1}(\mathbf{q}_0)(\breve{\mathbf{v}}_i - \mathbf{C}^T(\mathbf{q}_0)\breve{\boldsymbol{\zeta}}_i), \\
\breve{\mathbf{v}}'_i &= \mathbf{C}(\mathbf{q}_0)\mathbf{P}^{-1}(\mathbf{q}_0)(\breve{\mathbf{v}}_i - \mathbf{C}^T(\mathbf{q}_0)\breve{\boldsymbol{\zeta}}_i) + \mathbf{Q}(\mathbf{q}_0)\breve{\boldsymbol{\zeta}}_i - \mathbf{T}_i(\mathbf{q}_0), \\
f'_{ij} &= \boldsymbol{\zeta}_j^T \mathbf{T}_i(\mathbf{q}_0), \\
\breve{f}'_{ij} &= \breve{\boldsymbol{\zeta}}_j^T \mathbf{T}_i(\mathbf{q}_0),
\end{aligned}
\tag{18}
$$

with initial conditions

$$
\begin{aligned}
&\boldsymbol{\zeta}_i(0) = \mathbf{0}, \quad \mathbf{v}_i(0) = \mathbf{e}_i \quad i = 1, \ldots, p, \\
&\breve{\boldsymbol{\zeta}}_i(0) = \breve{\mathbf{v}}_i(0) = \mathbf{0}, \quad i = 1, \ldots, n, \\
&f_{ij}(0) = 0, \quad i = 1, \ldots, n, \quad j = 1, \ldots, p, \\
&\breve{f}_{ij}(0) = 0, \quad i, j = 1, \ldots, n.
\end{aligned}
$$

In the application that follows, before computing conjugate points, we determine $\mathbf{q}_0(s)$ by applying parameter continuation techniques and a collocation discretization (the package AUTO [7]) to a boundary value problem involving a Hamiltonian form of the Euler-Lagrange equations [18], and store the appropriate initial conditions for $\mathbf{q}_0$ and $\mathbf{q}'_0$. Then during the conjugate point computation, $\mathbf{q}_0$ is recovered by adjoining the Hamiltonian equations to the IVP system (18). Any other method for calculating and passing $\mathbf{q}_0(s)$ to the IVP system (18) could also be used.

4 The Elastic Rod Model of DNA Minicircles

4.1 Variational Principle

Our motivation for developing the isoperimetric conjugate point test was to determine stability in a twisted elastic rod model of DNA minicircles. In this section, we describe this rod theory and model the formation of a minicircle as an isoperimetric variational problem of the standard form (7). We adopt the special Cosserat theory of elastic rods, which is a standard model in continuum mechanics. We only provide a minimal outline of the material needed; a comprehensive discussion of the Cosserat theory can be found in [1], and the exact model and notation adopted here is more fully described in [16].

The configuration of an elastic rod is described by a centerline $\mathbf{r}(s)$ (written as a function of arclength s) and directors $\{\mathbf{d}_1(s), \mathbf{d}_2(s), \mathbf{d}_3(s)\}$ that form an orthonormal frame describing the orientation of the cross-section of the rod. For convenience, we choose a length-scale such that $0 \leq s \leq 1$. We restrict attention to inextensible and unshearable rods, for which $\mathbf{d}_3(s)$, the director perpendicular to the cross-section, coincides with the tangent vector to the centerline:

$$\mathbf{r}'(s) \equiv \frac{d\mathbf{r}(s)}{ds} = \mathbf{d}_3(s). \tag{19}$$

This assumption has been shown to be a rather good approximation for the DNA cyclization model presented here [18], because the forces involved are well below the threshold found by Bustamante [30] and others for significant DNA extension.

The stresses acting across a cross-section of the rod can be averaged to yield a net force $\mathbf{n}(s)$ and moment $\mathbf{m}(s)$ (of the material in $s+$ acting on the material in $s-$). The components

$$m_i(s) \equiv \mathbf{m}(s) \cdot \mathbf{d}_i(s), \quad i = 1, 2, 3,$$

of the moment $\mathbf{m}$ in the director frame play a role in a certain distinguished bifurcation diagram for rods (cf. Sec. 6); m_1 and m_2 are bending moments, and m_3 is the twisting moment.

Orthonormality of the directors $\{\mathbf{d}_i(s)\}$ implies the existence of a (Darboux) vector $\mathbf{u}(s)$ defined by the kinematic relations

$$\mathbf{d}_i'(s) = \mathbf{u}(s) \times \mathbf{d}_i(s), \qquad i = 1, 2, 3.$$

We denote the components of $\mathbf{u}$ in the rod frame by $u_i(s) \equiv \mathbf{u}(s) \cdot \mathbf{d}_i(s)$. The u_i are the *strains* in the model. Each orthonormal frame $\{\mathbf{d}_1(s), \mathbf{d}_2(s), \mathbf{d}_3(s)\}$

is an element of $SO(3)$, but rather than represent it by the traditional three Euler angles, we prefer instead to use a 4-vector of *Euler parameters* (or a *quaternion*) $\mathbf{q}(s)$. The Euler parameters provide the frame through the relations:

$$\mathbf{d}_1 = \frac{1}{|\mathbf{q}|^2}\begin{bmatrix} q_1^2 - q_2^2 - q_3^2 + q_4^2 \\ 2q_1q_2 + 2q_3q_4 \\ 2q_1q_3 - 2q_2q_4 \end{bmatrix}, \quad \mathbf{d}_2 = \frac{1}{|\mathbf{q}|^2}\begin{bmatrix} 2q_1q_2 - 2q_3q_4 \\ -q_1^2 + q_2^2 - q_3^2 + q_4^2 \\ 2q_2q_3 + 2q_1q_4 \end{bmatrix},$$
$$\mathbf{d}_3 = \frac{1}{|\mathbf{q}|^2}\begin{bmatrix} 2q_1q_3 + 2q_2q_4 \\ 2q_2q_3 - 2q_1q_4 \\ -q_1^2 - q_2^2 + q_3^2 + q_4^2 \end{bmatrix}. \tag{20}$$

The strains can then be expressed as (see e.g. [6])

$$u_i = \frac{2\,(\mathbf{q}')^T\,\mathbf{B}_i\mathbf{q}}{|\mathbf{q}|^2}, \tag{21}$$

where

$$\mathbf{B}_1 = \begin{bmatrix} 0 & 0 & 0 & 1 \\ 0 & 0 & 1 & 0 \\ 0 & -1 & 0 & 0 \\ -1 & 0 & 0 & 0 \end{bmatrix}, \ \mathbf{B}_2 = \begin{bmatrix} 0 & 0 & -1 & 0 \\ 0 & 0 & 0 & 1 \\ 1 & 0 & 0 & 0 \\ 0 & -1 & 0 & 0 \end{bmatrix}, \ \mathbf{B}_3 = \begin{bmatrix} 0 & 1 & 0 & 0 \\ -1 & 0 & 0 & 0 \\ 0 & 0 & 0 & 1 \\ 0 & 0 & -1 & 0 \end{bmatrix}. \tag{22}$$

A rod can have a nontrivial unstressed shape; that is, it may be curved and twisted even in the absence of external loads. This unstressed shape is specified by three functions $\hat{u}_1(s)$, $\hat{u}_2(s)$, and $\hat{u}_3(s)$, corresponding to the strains in the unstressed configuration. The local energy cost in deforming from this unstressed shape is given by a (material-dependent) strain energy density function E, whose integral over the length of the rod gives the total strain energy:

$$W \equiv \int_0^1 E(u_j - \hat{u}_j, s)\, ds.$$

Static equilibria of the rod are extremals of the strain energy functional W. One could assume a quite general dependence of E on the strains, but in our computations, we have specialized to a quadratic energy that has proven accurate for DNA minicircles [18]:

$$W \equiv \int_0^1 \left\{ \sum_{j=1}^{3} \frac{1}{2} K_j(s)[u_j - \hat{u}_j(s)]^2 \right\} ds. \tag{23}$$

Note that the integrand is a function of $(\mathbf{q}, \mathbf{q}', s)$, since the strains u_j are given by the relations (21). The positive *stiffness* functions $K_j(s)$ and the unstressed strains $\hat{u}_j(s)$ are required input parameters to the model.

Cyclization of DNA occurs when both the centerline and directors close:

$$\mathbf{r}(0) = \mathbf{r}(1), \quad \mathbf{d}_i(0) = \mathbf{d}_i(1). \tag{24}$$

However, it will be convenient to consider the more general problem in which the centerline $\mathbf{r}$ and tangent directors $\mathbf{d}_3$ close, but the normal directors $\mathbf{d}_1(0)$ and $\mathbf{d}_1(1)$ form an angle α as depicted in Fig. 1. The boundary conditions that describe the physical configuration illustrated in Fig. 1 are

$$\mathbf{r}(0) = \mathbf{r}(1) = \mathbf{0}, \quad \mathbf{q}(0) = \langle 0, 0, 0, 1\rangle, \quad \mathbf{q}(1) = \langle 0, 0, -\sin(\alpha/2), -\cos(\alpha/2)\rangle. \tag{25}$$

Note that the given functional W does not explicitly depend on $\mathbf{r}$ and $\mathbf{r}'$. In addition, the boundary conditions (25) on $\mathbf{r}$ can be transformed into an isoperimetric constraint on $\mathbf{q}(s)$ using condition (19):

$$\int_0^1 \mathbf{d}_3(\mathbf{q})\, ds = \int_0^1 \mathbf{r}'\, ds = \mathbf{r}(1) - \mathbf{r}(0) = \mathbf{0}. \tag{26}$$

Thus, the specific variational problem of the isoperimetric form (7) relevant for DNA minicircle formation is:

$$\begin{gathered} W = \int_0^1 \frac{1}{2} \left\{ \sum_{i=1}^{3} K_i(s) \Big[u_i(\mathbf{q}, \mathbf{q}') - \hat{u}_i(s) \Big]^2 \right\} ds, \\ \text{subject to} \quad \int_0^1 \mathbf{d}_3(\mathbf{q})\, ds = \mathbf{0}, \\ \mathbf{q}(0) = \langle 0, 0, 0, 1\rangle, \quad \mathbf{q}(1) = \langle 0, 0, -\sin(\alpha/2), -\cos(\alpha/2)\rangle. \end{gathered} \tag{27}$$

4.2 Applying the rod model to DNA

We now summarize the interpretation of an elastic rod as a model of DNA, as developed in [18]. A DNA molecule consists of two sugar-phosphate chains which wind around each other in a double helix, with cross-links called base-pairs that bind the two chains together. When an elastic rod model is adopted as a model of DNA, the centerline $\mathbf{r}(s)$ runs through the middle of the double helix, passing near the centers of the base-pairs, and the normal vector $\mathbf{d}_1(s)$ serves to locate the sugar-phosphate chains. Cyclization is the process by which the two ends of a single DNA molecule covalently bond to form a circular molecule, i.e., the boundary conditions (24) are satisfied. As mentioned above, it is computationally convenient to consider the more general boundary conditions (25).

In order to apply the rod model to DNA, one must determine from experimental data appropriate values for the stiffnesses K_i and the unstressed strains $\hat{u}_i$. This determination is the focus of an earlier study [18], whose results we summarize here.

Based on the best available measurements, the stiffnesses are assumed to be independent of s (although s-dependence could certainly be incorporated if improved experimental results become available). Furthermore we assume equal bending stiffnesses $K_1 = K_2$. This latter assumption may be at odds with chemical intuition of a preferred local bending direction. However, since the DNA is rapidly twisting (the sugar-phosphate chains make a full turn approximately every 10.5 base pairs), it can be shown that these unequal bending stiffnesses are averaged to give an effective isotropic rod on sufficiently large length scales [15].

The appropriate value of K_1 is generally agreed upon, based on sedimentation, light scattering, and cyclization experiments. With a scaling such that the DNA molecule has length one, the stiffness is [11]

$$K_1 = \frac{PRT}{N\ell},$$

where T is the temperature, $R = 8.314$ J/mol-Kelvin, $P \approx 463$ Å is the persistence length, $\ell \approx 3.4$ Å is the helix-rise-per-base-pair, and N is the number of base-pairs. The value of K_3 is more difficult to determine, and a range of values for the ratio $\gamma \equiv K_3/K_1$ appears in the literature (typically $0.5 \leq \gamma \leq 1.5$) [26]. The parameter continuation methods we employ make it straightforward to report results over this entire range of γ.

It is well known that certain DNA molecules have significantly curved unstressed shapes (e.g. sequences involving A-tracts), and ongoing computational and laboratory experiments can predict this unstressed shape given the underlying base-pair sequence. Appropriately filtering and smoothing this base-pair-level information allows us to determine slowly varying unstressed strains $\hat{u}_i(s)$ suitable for continuum rod computations [18].

Once K_i and $\hat{u}_i(s)$ are determined, computation of the equilibrium shapes of the cyclized DNA requires solving the Euler-Lagrange equations for the variational problem (27). Details of these computations can be found in [16] and [18]. The goal of this paper is to determine the isoperimetric index of each of these equilibria.

4.3 The Second Variation and Linearized Constraints

In order to determine the index, we first need to compute the specific form of the second variation (2) for the rod problem (27):

$$\delta^2 J[\boldsymbol{\zeta}] = \frac{1}{2}\int_0^1 \left[(\boldsymbol{\zeta}')^T L_{\mathbf{q}'\mathbf{q}'}\boldsymbol{\zeta}' + \boldsymbol{\zeta}^T L_{\mathbf{q}\mathbf{q}}\boldsymbol{\zeta} + \boldsymbol{\zeta}^T L_{\mathbf{q}\mathbf{q}'}\boldsymbol{\zeta}' \right.$$
$$\left. + (\boldsymbol{\zeta}')^T L_{\mathbf{q}'\mathbf{q}}\boldsymbol{\zeta} + \boldsymbol{\zeta}^T \left(\mathbf{g}_{\mathbf{q}\mathbf{q}}^T \boldsymbol{\lambda}_0\right)\boldsymbol{\zeta}\right]\, ds.$$

Using the chain rule on $L(\mathbf{q},\mathbf{q}') = E(u_i(\mathbf{q},\mathbf{q}') - \hat{u}_i)$, and applying (21), we find [23]

$$\begin{aligned} L_{\mathbf{qq}} \;=\; & \frac{4}{|\mathbf{q}|^4}\sum_{i,j=1}^{3} E_{u_iu_j}\Big[\mathbf{B}_i\mathbf{q}'\otimes\mathbf{B}_j\mathbf{q}' + u_j\mathbf{B}_i\mathbf{q}'\otimes\mathbf{q} + u_i\mathbf{q}\otimes\mathbf{B}_j\mathbf{q}' + u_iu_j\mathbf{q}\otimes\mathbf{q}\Big] \\ & + \frac{2}{|\mathbf{q}|^4}\sum_{i=1}^{3} m_i\Big[2\mathbf{B}_i\mathbf{q}'\otimes\mathbf{q} + 2\mathbf{q}\otimes\mathbf{B}_i\mathbf{q}' + 4u_i\mathbf{q}\otimes\mathbf{q} - |\mathbf{q}|^2u_i\mathbf{I}\Big], \end{aligned}$$

$$\begin{aligned} (L_{\mathbf{qq}'})^T = L_{\mathbf{q}'\mathbf{q}} \;=\; & -\frac{4}{|\mathbf{q}|^4}\sum_{i,j=1}^{3} E_{u_iu_j}\left[\mathbf{B}_i\mathbf{q}\otimes\mathbf{B}_j\mathbf{q}' + u_j\mathbf{B}_i\mathbf{q}\otimes\mathbf{q}\right] \\ & + \frac{2}{|\mathbf{q}|^4}\sum_{i=1}^{3} m_i\left[|\mathbf{q}|^2\mathbf{B}_i - 2\mathbf{B}_i\mathbf{q}\otimes\mathbf{q}\right], \end{aligned}$$

and

$$L_{\mathbf{q}'\mathbf{q}'} \;=\; \frac{4}{|\mathbf{q}|^4}\sum_{i,j=1}^{3} E_{u_iu_j}\mathbf{B}_i\mathbf{q}\otimes\mathbf{B}_j\mathbf{q},$$

where the $\mathbf{B}_i$ matrices are defined in (22) and $\otimes$ denotes the outer product. If we further assume that E is a quadratic function of the strains u_i as in (23), then

$$E_{u_iu_j} = K_i\delta_{ij}, \quad m_i = K_i(u_i - \hat{u}_i),$$

where δ_{ij} denotes the Kronecker delta.

It is easily seen from Eqs. (20) and (21) that the variational problem (27) is homogeneous in $\mathbf{q}$ (that is, it is invariant to the scaling $\mathbf{q}\to\alpha(s)\mathbf{q}$). Therefore, the second variation $\delta^2 J$ identically vanishes for variations of the form $\boldsymbol{\zeta} = \alpha(s)\mathbf{q}_0(s)$. These flat directions (which are artifacts of the four-parameter quaternion description of $SO(3)$) are of no interest in the determination of the index; thus we restrict our attention to variations $\boldsymbol{\zeta}$ in the subspace pointwise orthogonal to $\mathbf{q}_0(s)$ in $\mathbb{R}^4$. One basis for this subspace is $\{\mathbf{B}_1\mathbf{q}_0, \mathbf{B}_2\mathbf{q}_0, \mathbf{B}_3\mathbf{q}_0\}$ (cf. [6]). Hence we take $\boldsymbol{\zeta} = \boldsymbol{\Pi}\boldsymbol{\eta}$, where $\boldsymbol{\eta}(s)$ is a variation in $\mathbb{R}^3$ and

$$\boldsymbol{\Pi} = \begin{bmatrix}\mathbf{B}_1\mathbf{q}_0 & \mathbf{B}_2\mathbf{q}_0 & \mathbf{B}_3\mathbf{q}_0\end{bmatrix} \in \mathbb{R}^{4\times 3}.$$

The resulting second variation is

$$\delta^2 J[\boldsymbol{\eta}] = \frac{1}{2}\int_0^1 \left[(\boldsymbol{\eta}')^T\mathbf{P}\boldsymbol{\eta}' + \boldsymbol{\eta}^T\mathbf{C}\boldsymbol{\eta}' + (\boldsymbol{\eta}')^T\mathbf{C}^T\boldsymbol{\eta} + \boldsymbol{\eta}^T\mathbf{Q}\boldsymbol{\eta}\right] ds, \qquad (28)$$

where

$$\begin{aligned}
\mathbf{P} &= \mathbf{\Pi}^T L_{\mathbf{q}'\mathbf{q}'} \mathbf{\Pi}, \\
\mathbf{Q} &= (\mathbf{\Pi}')^T L_{\mathbf{q}'\mathbf{q}'} \mathbf{\Pi}' + \mathbf{\Pi}^T L_{\mathbf{q}\mathbf{q}} \mathbf{\Pi} + \mathbf{\Pi}^T \left(\mathbf{g}_{\mathbf{q}\mathbf{q}}^T \boldsymbol{\lambda}_0 \right) \mathbf{\Pi} + 2\mathbf{\Pi}^T L_{\mathbf{q}\mathbf{q}'} \mathbf{\Pi}', \\
\mathbf{C} &= (\mathbf{\Pi}')^T L_{\mathbf{q}'\mathbf{q}'} \mathbf{\Pi} + \mathbf{\Pi}^T L_{\mathbf{q}\mathbf{q}'} \mathbf{\Pi}.
\end{aligned} \tag{29}$$

Note that after projection by $\mathbf{\Pi}$, this second variation still takes the standard form (2). Further, for the energy (28), after projection, the resulting $\mathbf{P}$ is positive definite, whereas $L_{\mathbf{q}'\mathbf{q}'}$ alone is only positive semi-definite.

In addition to $\mathbf{P}$, $\mathbf{Q}$, and $\mathbf{C}$, the IVP (18) involves the linearization of the constraint $\int_0^1 \mathbf{d}_3(\mathbf{q})\, ds = \mathbf{0}$. In terms of the projected variations $\boldsymbol{\eta}$, the linearized constraint is:

$$\mathbf{T}_i = \mathbf{\Pi}^T \frac{\partial (\mathbf{d}_3 \cdot \mathbf{e}_i)}{\partial \mathbf{q}} (\mathbf{q}_0), \quad i = 1, 2, 3, \tag{30}$$

where $\mathbf{d}_3$ is given by (20).

5 Results

We are now in a position to implement the conjugate point test as described in Secs. 2 and 3 to the quadratic form (28) and constraints (30), so that $p = n = 3$. We solve the IVP system (18) numerically using an Adams-PECE adaptive step-size integrator [29], which takes approximately 10 seconds per equilibrium solution on a Dec Alpha 3000. (This time is somewhat inflated by the fact that our $\hat{u}_i$ functions are only C^1, which causes the adaptive-step-size integrator to take small steps in some regions; if $\hat{u}_i \in C^\infty$, the time per equilibrium drops to about 3 seconds.)

The value of $\det \mathbf{M}$ is evaluated on a grid of s values in $(0, 1)$ in order to track its zeroes (i.e., conjugate points). For example, Fig. 2 shows plots of $\det \mathbf{M}$ as a function of arclength for three equilibria. Since $\mathbf{M}(0)$ is the six-by-six zero matrix, $\det \mathbf{M}$ is very small for $s \approx 0$. In fact, asymptotic analysis of the entries in $\mathbf{M}$ (see Appendix B) demonstrates that:

$$\lim_{s \to 0} \frac{\det \mathbf{M}(s)}{s^{14}} = \frac{a_1^2 + a_2^2}{5 K_1^2 K_2^2 K_3} \equiv \Omega, \quad \text{where } a_i = \frac{\mathbf{e}_i^T \mathbf{q}_0'(0)}{576 \sqrt{K_i}}, \tag{31}$$

as verified in Fig. 3. This limit assures us that $\det \mathbf{M}(s) \neq 0$ for $s > 0$ sufficiently small, in agreement with the theory described in Sec. 2.

5.1 Code Validation

Our code was tested on an idealized problem with $\hat{u}_i(s) \equiv 0$ which has circular equilibria on which the isoperimetric index can be calculated analytically

[23, 24]. For non-planar equilibria of this idealized problem, stability exchanges can be shown to occur at folds in a certain distinguished diagram [24], as is further described in Sec. 6. Both of these analytic conclusions are reproduced by the conjugate point computations, which provides verification of our code [23], but we do not digress here to describe the details.

5.2 Stability Conclusions for DNA

We now present stability results for minicircle equilibria of a 150-base-pair DNA molecule that contains an A-tract with intrinsic bend of approximately 110 degrees, as well as other smaller sequence-induced bends (the molecule 05T05 described in [18]). The set of equilibria as the angle α is varied lie on several different components; the two lowest-energy components are shown in Fig. 4 for $\gamma = K_3/K_1 = 1.7$. The results of the stability computations are represented by the line styles in the bifurcation diagrams, which denote the isoperimetric index of the energy functional (23). For this particular value of γ (which is slightly above the range of generally accepted values for DNA), the entire low-energy component is stable, while the other component is entirely unstable, but of varying isoperimetric index.

The true cyclized equilibria (those with closed centerlines *and* closed double-helices) are labeled with circles in Fig. 4. There are two such equilibria on the low-energy component, labeled a and b, and their physical configurations are shown in Fig. 5. The other component also contains several cyclized equilibria (and indeed there are many more on higher-energy components not shown here), but none are stable, and hence will presumably not be seen experimentally. However, when self-contact forces are added to the model, some of these higher-energy cyclized equilibria may be stabilized.

For all values of γ studied, the higher-energy component is entirely unstable, so it will not be displayed further. However, the stability properties of the lower-energy component do change with γ and merit discussion. This lower energy component is shown in Fig. 6 for three values of γ, with the cyclized equilibria again marked with circles and labeled as in Fig. 4. Note the appearance of a region of instability at the top of the diagram, but that the two equilibria labeled a and b remain stable throughout. In addition, if γ is sufficiently small, two new cyclized equilibria emerge, one stable (labeled d) and one unstable (labeled e).

6 Discussion

We have exploited ideas from an index theory for the second variation in the unconstrained calculus of variations to derive an isoperimetric index pertinent to constrained calculus of variations problems. The isoperimetric

index is the number of constrained conjugate points along an extremal, and also characterizes the maximal dimension of a subspace of admissible variations on which the constrained second variation can be made negative. In addition, we described a practical numerical implementation for determining the isoperimetric index based on a count of the number of zeroes of the determinant of a certain constrained stability matrix. In particular, when the determinant is of constant sign along the extremal, the isoperimetric index is zero and the constrained second variation is non-negative. The absence of a constrained conjugate point (in the sense we use) was previously described by Bolza [4] as a necessary and sufficient condition for the second variation to be nonnegative. However, we believe the connection between constrained conjugate points and a projected eigenvalue problem, which is the viewpoint that allows a definition of the isoperimetric index, to be a new observation. In any case, the test of Bolza is apparently not widely disseminated in the contemporary literature, although it has been exploited by Benjamin [2] and Segercrantz [28].

We remark that in the isoperimetric case, there is a surprisingly sparse literature on when second-variation tests provide *sufficient* conditions for a constrained extremal to be a local minimum. Vogel [31] addresses the case of a single constraint.

We applied our theory to calculate the isoperimetric index of families of critical points in an example arising in the modeling of DNA minicircles. In this problem the variational principle involves an internal or potential energy, so those critical points that realize a constrained local minimum can be anticipated to be physically stable configurations that should be observable in experiment. The analysis developed here reveals that for the 11 DNA molecules considered in [18] there are always at least two local minima, i.e. critical points with isoperimetric index zero.

In a more speculative vein, we believe that critical points of the DNA variational principle with non-zero isoperimetric index may also be of physical interest. The families of critical points shown in Fig. 4 include branches of trefoil-like solutions approaching self-intersection with isoperimetric index at least two. Macroscopic experiments with twisted elastic wires reveal that when effects of self-contact are included, some trefoil-like configurations are physically stable. Thus it seems likely that the isoperimetric index computed here will be one ingredient in a stability analysis of critical points in a more sophisticated model encompassing effects of self-contact.

The fact that the isoperimetric calculus of variations problem arising in our DNA model involves a parameter α that can be varied continuously to generate families of critical points (cf. Figs. 4 and 6) invites comparison between our isoperimetric conjugate point theory and various principles of exchange of stability in bifurcation and continuation problems. Under certain genericity assumptions, it is a standard result of bifurcation theory

that stability of equilibria will change as a branch of solutions is traversed through a fold (i.e. a local minimum or maximum of the parameter). We now demonstrate that this conclusion is consistent with the constrained conjugate point theory developed here. We consider the parameter α and the equilibria $(\mathbf{q}_0, \boldsymbol{\lambda}_0)$ as functions of a 'pseudo-arclength' τ [7] which varies monotonically along a segment of a computed branch with a fold in the parameter α. Then $\dot{\alpha} = 0$ at the fold point. When the Euler-Lagrange equations, boundary conditions, and integral constraints are differentiated with respect to τ, we see that whenever $\dot{\alpha} = 0$, the conjugate point equations (9) have a nontrivial solution with $\sigma = 1$. Thus we conclude that at fold points a new conjugate point may enter or leave the interval $(0, 1)$, consistent with traditional stability exchange theory.

For parameter dependent variational principles, the standard stability exchange results can be strengthened to predict the direction of stability exchange at a fold from the shape of the solution branch in certain distinguished diagrams [17, 24]. For the DNA example, a distinguished diagram is provided by a plot of twist moment m_3 versus angle α, and the direction of stability exchange is as depicted in Fig. 7. Fig. 8 illustrates this distinguished projection of the solution branches previously shown in Fig. 6. The changes in isoperimetric index computed with the constrained conjugate point test agree with the index exchange predictions of distinguished diagram theory. While distinguished diagrams provide a convenient framework for summarizing and understanding index changes, they do not provide an alternative to explicit calculation of conjugate points for two reasons. First, the distinguished diagram can only predict changes in isoperimetric index, so that the index of at least one critical point in each connected component of solutions must be determined by some other means. Second, as in the standard exchange of stability theory, predictions from a distinguished diagram depend upon certain genericity assumptions (e.g. simplicity of folds). The constrained conjugate point test presented here is a direct computation of the isoperimetric index that is not subject to either of these limitations. In fact the two approaches yield an efficacious combination of conclusions.

Bifurcation diagrams with the angle α plotted as abscissa (for example Fig. 8) clarify the genesis of the two additional cyclized equilibria that was observed in Sec. 5: as the parameter γ is lowered the solution branch folds back on itself to cross $\alpha = 0$, once with α decreasing, and then later with α increasing. As γ is lowered further, more cyclized equilibria can be created as the diagram is further stretched laterally.

Finally, we remark on the holonomy, i.e. discontinuous behavior, of the angle α that is revealed in Fig. 8. Although the equilibria labeled b at the left and right ends of each curve are exactly the same physical solution, the value of the angle α has been increased by 4π as the branch of critical points is traversed. This numerically observed behavior was counter-intuitive for

us: one can track a branch of equilibria as α is increased monotonically (as in the case $\gamma = 1.7$) and yet still return to the original configuration b. However there is no contradiction once two observations are made. First the angle between the directors $\mathbf{d}_1(1)$ and $\mathbf{d}_1(0)$ is only defined mod 2π (and the associated quaternion parameterization we exploit is only defined mod 4π). Second, provided that the centerline of the rod self-intersects in at least one of the equilibria in the branch of solutions, there is no way to construct a contradiction based upon a continuity argument involving angle as a function of arc-length. As remarked above, the rod model described in Sec. 4 does not account for self-contact, so that the rod may pass through itself without penalty. Our computations show that the rod does self-intersect at least once as each connected component of the solution set is traversed.

The holonomy in angle allows there to be an entire closed curve of equilibria all of which are stable, since the angle α does not fold (e.g. when $\gamma = 1.7$). Generally, one would expect any closed curve of equilibria (or an *isola*) to contain at least one segment of unstable solutions, since all quantities must fold at least once in order to return to their original values, and hence stability exchange will occur. It is only because of the holonomy of the parameter α that there can be an isola consisting entirely of stable equilibria.

Acknowledgments: RSM was supported by an NSF Postdoctoral Research Fellowship and the AFOSR; KAR by an ONR AASERT Award; and JHM by the AFOSR and ONR. It is a pleasure to thank Professors R. Pego and L. Greenberg for helpful discussions, and the referees for several useful suggestions.

A Properties of the eigenvalue problem (11)

In this appendix we prove that the spectrum of the projected eigenvalue problem (11) satisfies Properties 1–3. To begin, we denote the Sobolev space of functions with weak second derivatives on the interval $(0, \sigma)$ by $\mathcal{A}(\sigma)$, and define:

$$\mathcal{A}_d(\sigma) \equiv \{\boldsymbol{\zeta} \in \mathcal{A}(\sigma) : \boldsymbol{\zeta}(0) = \boldsymbol{\zeta}(\sigma) = \mathbf{0}\}.$$

It is typical in the unconstrained calculus of variations to study the densely-defined operator $\mathcal{S} : \mathcal{A}_d(\sigma) \subset L^2(0,\sigma) \to L^2(0,\sigma)$ (see e.g. [13, p. 262]). In the isoperimetric case, we further define the spaces:

$$\begin{aligned} \mathcal{T} &\equiv \text{span}(\mathbf{T}_1, \cdots, \mathbf{T}_n), \\ \mathcal{T}^\perp(\sigma) &\equiv \{\boldsymbol{\zeta} \in L^2(0,\sigma) : \int_0^\sigma \boldsymbol{\zeta}^T \mathbf{T}_i \, ds = 0, \;\; i = 1, \cdots, n\}, \\ \mathcal{A}_d^{cons}(\sigma) &\equiv \mathcal{A}_d(\sigma) \cap \mathcal{T}^\perp(\sigma). \end{aligned}$$

Throughout this section, we consider the densely-defined operator $\mathcal{Q}\mathcal{S}\mathcal{Q} : \mathcal{A}_d^{cons}(\sigma) \subset \mathcal{T}^\perp(\sigma) \to \mathcal{T}^\perp(\sigma)$. When $\sigma = 1$, $\mathcal{A}_d(\sigma)$ and $\mathcal{A}_d^{cons}(\sigma)$ are identical to the spaces $\mathcal{A}_d$ and $\mathcal{A}_d^{cons}$ as defined in Sec. 2.

As described in Sec. 2.2, an isoperimetric conjugate point is defined to be a value $\sigma < 1$ for which there is a nontrivial solution to

$$\mathcal{Q}\mathcal{S}\mathcal{Q}\boldsymbol{\zeta} = \mathbf{0}, \quad 0 < s < \sigma, \;\; \boldsymbol{\zeta} \in \mathcal{A}_d^{cons}(\sigma), \tag{32}$$

where $\mathcal{Q}(\sigma)$ is the (self-adjoint) orthogonal projection from the Hilbert space $L^2(0,\sigma)$ onto its subspace $\mathcal{T}^\perp(\sigma)$, i.e.

$$\mathcal{Q}\boldsymbol{\zeta} = \boldsymbol{\zeta} - \sum_{i,j=1}^{n} \mathbf{T}_i \beta_{ij} \int_0^\sigma \boldsymbol{\zeta}^T \mathbf{T}_j, \tag{33}$$

where the matrix $\boldsymbol{\beta} = \{\beta_{ij}\}$ is defined by $\boldsymbol{\beta}^{-1} \equiv \{\int_0^\sigma \mathbf{T}_i^T \mathbf{T}_j \; ds\}$. (The matrix $\boldsymbol{\beta}$ is invertible by virtue of the linear independence assumption on the $\mathbf{T}_i$.) Note that by construction $\mathcal{T}^\perp(\sigma)$ has finite codimension in $L^2(0,\sigma)$.

Since $\mathcal{Q}\boldsymbol{\zeta} = \boldsymbol{\zeta}$ for $\boldsymbol{\zeta} \in \mathcal{A}_d^{cons}(\sigma)$, the operator in Eq. (32) could be written as $\mathcal{Q}\mathcal{S}$, but we retain the notation $\mathcal{Q}\mathcal{S}\mathcal{Q}$ to emphasize self-adjointness. It is important that the domain in (32) be the constrained space $\mathcal{A}_d^{cons}(\sigma)$. If one were to work in the unconstrained space $\mathcal{A}_d(\sigma)$, then our choice of projection would be problematic, since $\mathcal{Q}\boldsymbol{\zeta}$ would not then respect the required boundary conditions. One could perhaps proceed using a projection from $\mathcal{A}_d(\sigma)$ to $\mathcal{A}_d^{cons}(\sigma)$, however in our experience the projection (33) and the conjugate point definition (32) is the most efficacious combination for defining an index.

We now proceed to prove Properties 1–3 described in Sec. 2.1 for the constrained eigenvalue problem:

$$\mathcal{QSQ}\boldsymbol{\zeta} = \rho(\sigma)\boldsymbol{\zeta}, \quad 0 < s < \sigma, \;\; \boldsymbol{\zeta} \in \mathcal{A}_d^{cons}(\sigma). \tag{34}$$

Property 1: The spectrum of the operator $\mathcal{QSQ} : \mathcal{A}_d^{cons}(\sigma) \subset \mathcal{T}^\perp \rightarrow \mathcal{T}^\perp$ consists of isolated eigenvalues $\rho_1(\sigma) \leq \rho_2(\sigma) \leq \cdots$ each with finite (geometric) multiplicity.

Proof: The property as stated is equivalent to the condition that the self-adjoint operator $\mathcal{QSQ}$ have no essential spectrum.[7] Assume that ρ is in the essential spectrum of $\mathcal{QSQ}$. Then it follows [3, p. 206] that there exists a sequence $\boldsymbol{\zeta}_j \in \mathcal{A}_d^{cons}(\sigma)$ with:

$$\begin{aligned}
&a)\ \inf_j \|\boldsymbol{\zeta}_j\| > 0, \\
&b)\ \lim_{j\rightarrow\infty} \int_0^\sigma \boldsymbol{\zeta}_j^T\, \mathbf{h}\, ds = 0, \;\; \forall\, \mathbf{h} \in \mathcal{T}^\perp \;\; \text{(weak convergence of } \boldsymbol{\zeta}_j \text{ to } \mathbf{0}), \\
&c)\ (\mathcal{QSQ} - \rho\mathcal{I})\boldsymbol{\zeta}_j \rightarrow \mathbf{0} \;\; \text{(strong convergence to } \mathbf{0} \text{ in } L^2(0,\sigma)).
\end{aligned} \tag{35}$$

Any $\boldsymbol{\chi} \in L^2(0,\sigma)$ can be written as $\boldsymbol{\chi} = \mathbf{h} + \mathbf{t}$ for $\mathbf{h} \in \mathcal{T}^\perp(\sigma)$ and $\mathbf{t} \in \mathcal{T}$. Further,

$$\int_0^\sigma \boldsymbol{\zeta}_j^T \boldsymbol{\chi} ds = \int_0^\sigma \boldsymbol{\zeta}_j^T \mathbf{h} ds,$$

since $\boldsymbol{\zeta}_j \in \mathcal{A}_d^{cons}(\sigma)$. Thus, we can strengthen part (b) of Eq. (35):

$$\lim_{j\rightarrow\infty} \int_0^\sigma \boldsymbol{\zeta}_j^T \boldsymbol{\chi} ds = 0, \; \forall \boldsymbol{\chi} \in L^2(0,\sigma).$$

Next, we can rewrite

$$\mathcal{QSQ} - \rho\mathcal{I} = (\mathcal{S} - \rho\mathcal{I}) + \mathcal{F}, \tag{36}$$

where $\mathcal{F} = (-\mathcal{PS} - \mathcal{SP} + \mathcal{PSP})$ has finite dimensional range, namely $\{\mathcal{T}, \mathcal{ST}\}$. Thus $\mathcal{F}$ is a compact operator, and hence transforms the weakly convergent sequence $\boldsymbol{\zeta}_j$ into a strongly convergent sequence [3, p. 39], i.e. $\mathcal{F}\boldsymbol{\zeta}_j \rightarrow \mathbf{0}$. Accordingly, using Eqs. (36) and part (c) of (35), we have $(\mathcal{S} - \rho\mathcal{I})\boldsymbol{\zeta}_j \rightarrow \mathbf{0}$. Thus we have shown that there exists a sequence $\boldsymbol{\zeta}_j \in \mathcal{A}_d^{cons}(\sigma) \subset \mathcal{A}_d(\sigma)$ such that:

$$\begin{aligned}
&a)\ \inf_j \|\boldsymbol{\zeta}_j\| > 0, \\
&b)\ \lim_{j\rightarrow\infty} \int_0^\sigma \boldsymbol{\zeta}_j^T\, \boldsymbol{\chi}\, ds = 0, \;\; \forall\, \boldsymbol{\chi} \in L^2(0,\sigma), \\
&c)\ (\mathcal{S} - \rho\mathcal{I})\boldsymbol{\zeta}_j \rightarrow 0.
\end{aligned} \tag{37}$$

[7] There is some variation in how the essential spectrum is defined. Here we take the definition set forth in [3].

or equivalently that the Sturm-Liouville operator $\mathcal{S} : \mathcal{A}_d(\sigma) \subset L^2(0,\sigma) \to L^2(0,\sigma)$ has ρ as part of its essential spectrum. However, under the standard assumption that $\mathbf{P}$ is positive definite, which is true for the rod model (see Appendix B), it is well-known that $\mathcal{S}$ has no essential spectrum (see, e.g. [22]). Thus, we arrive at a contradiction and conclude that the essential spectrum of $\mathcal{QSQ}$ must be empty. $\square$

In order to introduce a Rayleigh quotient characterization of eigenvalues, we denote the L^2-orthonormal eigenfunctions of (34) by $\boldsymbol{\zeta}_i(s;\sigma)$ and define the following sequence of spaces:

$$\mathcal{B}_1(\sigma) \equiv \mathcal{A}_d^{cons}(\sigma),$$
$$\mathcal{B}_m(\sigma) \equiv \left\{ \boldsymbol{\zeta} \in \mathcal{A}_d^{cons}(\sigma) : \int_0^\sigma \boldsymbol{\zeta}^T \boldsymbol{\zeta}_1 \, ds = \cdots = \int_0^\sigma \boldsymbol{\zeta}^T \boldsymbol{\zeta}_{m-1} \, ds = 0 \right\}, \quad m > 1.$$

Property 2: Each eigenvalue $\rho_j(\sigma)$ is a monotonically decreasing function of σ.

Proof: The operator $\mathcal{QSQ} : \mathcal{A}_d^{cons}(\sigma) \subset \mathcal{T}^\perp(\sigma) \to \mathcal{T}^\perp(\sigma)$ is self-adjoint, linear, bounded below, and obeys Property 1. Further, $\mathcal{A}_d^{cons}(\sigma)$ is dense in $\mathcal{T}^\perp(\sigma)$ (using Lemma 1 on p. 184 of [32] along with the standard fact that $\mathcal{A}_d(\sigma)$ is dense in $L^2(0,\sigma)$). Therefore, the eigenvalues $\rho_j(\sigma)$ are given by a variational principle [32, p. 6]:

$$\rho_m(\sigma) = \min_{\boldsymbol{\zeta} \in \mathcal{B}_m(\sigma)} \frac{\int_0^\sigma \boldsymbol{\zeta}^T \mathcal{QSQ} \boldsymbol{\zeta} \, ds}{\int_0^\sigma \boldsymbol{\zeta}^T \boldsymbol{\zeta} \, ds}. \tag{38}$$

Consider $\sigma_1 < \sigma_2$. Let the functions $\boldsymbol{\psi}_i(s), \quad i = 1, \ldots, m$ be defined on $0 \le s \le \sigma_2$ by:

$$\boldsymbol{\psi}_i(s) \equiv \begin{cases} \boldsymbol{\zeta}_i(s;\sigma_1) & 0 \le s \le \sigma_1, \\ \mathbf{0} & \sigma_1 < s \le \sigma_2. \end{cases}$$

Now determine a nontrivial linear combination $\sum_{k=1}^m a_k \boldsymbol{\psi}_k(s)$ which is orthogonal to every element of $\mathrm{span}(\boldsymbol{\zeta}_1(s;\sigma_2), \cdots, \boldsymbol{\zeta}_{m-1}(s;\sigma_2))$, and hence an element of $\mathcal{B}_m(\sigma_2)$:

$$\begin{bmatrix} \int_0^{\sigma_2} \boldsymbol{\zeta}_1^T \boldsymbol{\psi}_1 & \int_0^{\sigma_2} \boldsymbol{\zeta}_1^T \boldsymbol{\psi}_2 & \cdots & \int_0^{\sigma_2} \boldsymbol{\zeta}_1^T \boldsymbol{\psi}_m \\ \int_0^{\sigma_2} \boldsymbol{\zeta}_2^T \boldsymbol{\psi}_1 & \int_0^{\sigma_2} \boldsymbol{\zeta}_2^T \boldsymbol{\psi}_2 & \cdots & \int_0^{\sigma_2} \boldsymbol{\zeta}_2^T \boldsymbol{\psi}_m \\ \vdots & \vdots & \ddots & \vdots \\ \int_0^{\sigma_2} \boldsymbol{\zeta}_{m-1}^T \boldsymbol{\psi}_1 & \int_0^{\sigma_2} \boldsymbol{\zeta}_{m-1}^T \boldsymbol{\psi}_2 & \cdots & \int_0^{\sigma_2} \boldsymbol{\zeta}_{m-1}^T \boldsymbol{\psi}_m \end{bmatrix} \begin{bmatrix} a_1 \\ a_2 \\ \vdots \\ \vdots \\ a_m \end{bmatrix} = \mathbf{0}. \tag{39}$$

Since the matrix in (39) has more columns than rows, a nontrivial solution always exists. For convenience, we rescale so that $\sum_{k=1}^m a_k^2 = 1$.

Inserting $\boldsymbol{\zeta} = \sum_{k=1}^m a_k \boldsymbol{\psi}_k(s)$ into (38), we have:

$$\rho_m(\sigma_2) \leq \frac{\int_0^{\sigma_2} \left[\sum_{i=1}^m a_i \boldsymbol{\psi}_i(s)\right]^T \mathcal{Q}(\sigma_2)\mathcal{S}\mathcal{Q}(\sigma_2) \left[\sum_{k=1}^m a_k \boldsymbol{\psi}_k(s)\right]\, ds}{\int_0^{\sigma_2} \left[\sum_{i=1}^m a_i \boldsymbol{\psi}_i(s)\right]^T \left[\sum_{k=1}^m a_k \boldsymbol{\psi}_k(s)\right]\, ds}. \tag{40}$$

Now, since $\boldsymbol{\psi}_i \in \mathcal{A}_d^{cons}(\sigma_2)$, we have $\mathcal{Q}(\sigma_2)\boldsymbol{\psi}_i = \boldsymbol{\psi}_i$, so that the projections may be removed from (40):

$$\rho_m(\sigma_2) \leq \frac{\int_0^{\sigma_2} \left[\sum_{i=1}^m a_i \boldsymbol{\psi}_i(s)\right]^T \mathcal{S} \left[\sum_{k=1}^m a_k \boldsymbol{\psi}_k(s)\right]\, ds}{\int_0^{\sigma_2} \left[\sum_{i=1}^m a_i \boldsymbol{\psi}_i(s)\right]^T \left[\sum_{k=1}^m a_k \boldsymbol{\psi}_k(s)\right]\, ds}.$$

Both integrands vanish for $\sigma_1 < s < \sigma_2$, so we may change the upper integration limits to σ_1 and replace ψ_i by its restriction to $(0, \sigma_1)$:

$$\rho_m(\sigma_2) \leq \frac{\int_0^{\sigma_1} \left[\sum_{i=1}^m a_i \boldsymbol{\zeta}_i(s;\sigma_1)\right]^T \mathcal{S} \left[\sum_{k=1}^m a_k \boldsymbol{\zeta}_k(s;\sigma_1)\right]\, ds}{\int_0^{\sigma_1} \left[\sum_{i=1}^m a_i \boldsymbol{\zeta}_i(s;\sigma_1)\right]^T \left[\sum_{k=1}^m a_k \boldsymbol{\zeta}_k(s;\sigma_1)\right]\, ds}.$$

Next, we use the fact that $\mathcal{Q}(\sigma_1)\boldsymbol{\zeta}_i(s;\sigma_1) = \boldsymbol{\zeta}_i(s;\sigma_1)$ to introduce $\mathcal{Q}(\sigma_1)$ on either side of $\mathcal{S}$ and then exploit the fact that $\{\boldsymbol{\zeta}_i(s;\sigma_1)\}$ is a set of orthonormal eigenfunctions of $\mathcal{Q}(\sigma_1)\mathcal{S}\mathcal{Q}(\sigma_1)$ to find:

$$\rho_m(\sigma_2) \leq \frac{\sum_{i,k=1}^m a_i a_k \rho_k(\sigma_1)\delta_{ik}}{\sum_{i=1}^m a_i^2} = \sum_{i=1}^m a_i^2 \rho_i(\sigma_1) \leq \rho_m(\sigma_1).$$

□

Now we rewrite (34) in a form more useful for computation:

Lemma 1: For $\boldsymbol{\zeta} \in \mathcal{A}_d^{cons}(\sigma)$,

$$\mathcal{Q}\mathcal{S}\mathcal{Q}\boldsymbol{\zeta} = \rho\boldsymbol{\zeta} \iff \mathcal{S}\boldsymbol{\zeta} - \rho\boldsymbol{\zeta} \in \mathcal{T}.$$

Proof: The equation $\mathcal{Q}\mathcal{S}\mathcal{Q}\boldsymbol{\zeta} = \rho\boldsymbol{\zeta}$ is equivalent to $\mathcal{Q}\mathcal{S}\boldsymbol{\zeta} = \rho\mathcal{Q}\boldsymbol{\zeta}$ since $\mathcal{Q}$ is the identity on $\mathcal{A}_d^{cons}(\sigma)$. We can rearrange this to the form $\mathcal{Q}(\mathcal{S}\boldsymbol{\zeta} - \rho\boldsymbol{\zeta}) = \mathbf{0}$, which is true if and only if $\mathcal{S}\boldsymbol{\zeta} - \rho\boldsymbol{\zeta} \in \mathcal{T}$, since $\mathcal{T}$ is the kernel of $\mathcal{Q}$.

□

Property 3: For σ sufficiently close to 0, $\rho_j(\sigma) > 0,\ \forall j$.

Proof: Standard unconstrained quadratic form theory for Sturm-Liouville operators (see for example [27]) allows us to conclude that for σ sufficiently small,

$$\int_0^\sigma \boldsymbol{\zeta}^T(s)\mathcal{S}(s)\boldsymbol{\zeta}(s)\, ds > 0, \quad \forall \boldsymbol{\zeta} \in \mathcal{A}_d(\sigma).$$

Using Lemma 1, we know that ρ_j satisfies $S\boldsymbol{\zeta}_j - \rho_j \boldsymbol{\zeta}_j \in \mathcal{T}$ for $\boldsymbol{\zeta}_j \in \mathcal{A}_d^{cons}(\sigma)$. Premultiplying this expression by $\boldsymbol{\zeta}_j^T$ and integrating from 0 to σ, we see that for sufficiently small σ, $\rho_j(\sigma) > 0$, $\forall j$. □

Lemma 2: For a given extremal $\mathbf{q}_0$, the isoperimetric index equals the largest dimension of a subspace of $\mathcal{A}_d^{cons}(1)$ on which $\delta^2 J[\boldsymbol{\zeta}] = \int_0^1 \boldsymbol{\zeta}^T \mathcal{S} \boldsymbol{\zeta}\, ds$ is negative.

Proof: If the isoperimetric index is denoted by I, then $\rho_j(1) < 0$ for $j \leq I$ and $\rho_{I+1}(1) \geq 0$. Since $\mathcal{Q}(1)$ is the identity on $\mathcal{A}_d^{cons}(1)$, the lowest I eigenvectors $\boldsymbol{\zeta}_i(s;1)$ of $\mathcal{QSQ}$ provide a subspace of $\mathcal{A}_d^{cons}(1)$ on which $\delta^2 J < 0$, since:

$$\int_0^1 \boldsymbol{\zeta}_i^T \mathcal{S} \boldsymbol{\zeta}_j \, ds = \int_0^1 \boldsymbol{\zeta}_i^T \mathcal{QSQ} \boldsymbol{\zeta}_j \, ds = \rho_i(1) \delta_{ij}.$$

Suppose now that there exists an $(I+1)$-dimensional subspace $\mathcal{C}_{neg}$ of $\mathcal{A}_d^{cons}(1)$ on which $\delta^2 J < 0$. We invoke an alternative variational expression for the eigenvalues of $\mathcal{QSQ}$, the Fischer-Pólya minimax characterization [32, p. 12]. With $\mathcal{C}$ denoting an arbitrary $(I+1)$-dimensional subspace of $\mathcal{A}_d^{cons}(1)$, we have

$$\begin{aligned} \rho_{I+1}(1) = \min_{\mathcal{C}} \max_{\substack{\boldsymbol{\chi} \in \mathcal{C} \\ |\boldsymbol{\chi}|=1}} \int_0^1 \boldsymbol{\chi}^T \mathcal{QSQ} \boldsymbol{\chi} \, ds &= \min_{\mathcal{C}} \max_{\substack{\boldsymbol{\chi} \in \mathcal{C} \\ |\boldsymbol{\chi}|=1}} \int_0^1 \boldsymbol{\chi}^T \mathcal{S} \boldsymbol{\chi} \, ds \\ &\leq \max_{\substack{\boldsymbol{\chi} \in \mathcal{C}_{neg} \\ |\boldsymbol{\chi}|=1}} \int_0^1 \boldsymbol{\chi}^T \mathcal{S} \boldsymbol{\chi} \, ds = \max_{\substack{\boldsymbol{\chi} \in \mathcal{C}_{neg} \\ |\boldsymbol{\chi}|=1}} \delta^2 J[\boldsymbol{\chi}]. \end{aligned}$$

The unit sphere in the finite-dimensional $\mathcal{C}_{neg}$ is compact, so the maximum is attained at some $\boldsymbol{\chi}^* \in \mathcal{C}_{neg}$. Thus, we have:

$$\rho_{I+1}(1) \leq \delta^2 J[\boldsymbol{\chi}^*] < 0,$$

since by supposition $\delta^2 J < 0$ on $\mathcal{C}_{neg}$. This contradicts the known non-negativity of $\rho_{I+1}(1)$ and thus proves that there can be no subspace of dimension $I+1$ on which $\delta^2 J < 0$. □

B Asymptotic Analysis of $\det \mathbf{M}$

To better understand the behavior of the determinant of the constrained stability matrix $\mathbf{M}$ near $s = 0$, we study the asymptotic behavior of the entries of $\mathbf{M}$. First, we require the asymptotic expansion of $\mathbf{q}_0(s)$ for s small; for ease of notation, $\mathbf{q}_0$ will simply be denoted by $\mathbf{q}$ throughout this appendix. Boundary conditions ensure that $\mathbf{q}(0) = \langle 0, 0, 0, 1 \rangle$. The

constraint $|\mathbf{q}(s)| = 1$ implies $\mathbf{q}(0)^T\mathbf{q}'(0) = 0$, which implies $q_4'(0) = 0$. The other three components of $\mathbf{q}'(0)$ will in general be non-zero, and their values can not be determined *a priori*; one must extract them from the equilibrium solution. We have $\mathbf{q}'(0) = \langle q_1'(0), q_2'(0), q_3'(0), 0\rangle$, which implies that for small s:

$$\mathbf{q}'(s) = \begin{bmatrix} q_1'(0) \\ q_2'(0) \\ q_3'(0) \\ 0 \end{bmatrix} + O(s),$$

where the notation $O(s)$ denotes terms of order s or higher. Integrating (and recalling that $\mathbf{q}(0) = \langle 0, 0, 0, 1\rangle$), we find that for small s:

$$\mathbf{q}(s) = \begin{bmatrix} q_1'(0)s \\ q_2'(0)s \\ q_3'(0)s \\ 1 \end{bmatrix} + O(s^2).$$

Using the definition of $\mathbf{T}_i$ in Eq. (30), along with Eq. (20), we find that for small s:

$$\mathbf{T}_1(s) = \begin{bmatrix} 4q_3'(0)s + O(s^2) \\ 2 + O(s^2) \\ 0 \end{bmatrix}, \mathbf{T}_2(s) = \begin{bmatrix} -2 + O(s^2) \\ 4q_3'(0)s + O(s^2) \\ 0 \end{bmatrix},$$
$$\mathbf{T}_3(s) = \begin{bmatrix} -4q_1'(0)s + O(s^2) \\ -4q_2'(0)s + O(s^2) \\ 0 \end{bmatrix}. \tag{41}$$

The third components are zero for all s, so no asymptotic expansion is required.

We can now determine the asymptotic behaviors of the elements of $\mathbf{M}$. To begin, we consider the second-order operator $\mathcal{S}$:

$$\mathcal{S}\boldsymbol{\zeta} = -\frac{d}{ds}\left[\mathbf{P}\boldsymbol{\zeta}' + \mathbf{C}^T\boldsymbol{\zeta}\right] + \mathbf{C}\boldsymbol{\zeta}' + \mathbf{Q}\boldsymbol{\zeta},$$

where the coefficients $\mathbf{P}$, $\mathbf{C}$, and $\mathbf{Q}$ are given in Eq. (29). By direct computation:

$$\mathbf{P} = \begin{bmatrix} 4K_1 & 0 & 0 \\ 0 & 4K_2 & 0 \\ 0 & 0 & 4K_3 \end{bmatrix},$$
$$\mathbf{C} = \begin{bmatrix} 0 & 4K_2u_3 - 2m_3 & -4K_3u_2 + 2m_2 \\ -4K_1u_3 + 2m_3 & 0 & 4K_3u_1 - 2m_1 \\ 4K_1u_2 - 2m_2 & -4K_2u_1 + 2m_1 & 0 \end{bmatrix}.$$

Since $\mathbf{P}$ is independent of s, we rewrite $\mathcal{S}$ as:

$$\mathcal{S}\boldsymbol{\zeta} = -\mathbf{P}\boldsymbol{\zeta}'' - (\mathbf{C}')^T\boldsymbol{\zeta} + (\mathbf{C} - \mathbf{C}^T)\boldsymbol{\zeta}' + \mathbf{Q}\zeta.$$

We now consider the initial value problem which determines $\boldsymbol{\zeta}_i(s)$:

$$\mathcal{S}\boldsymbol{\zeta}_i = \mathbf{0},\ \boldsymbol{\zeta}_i(0) = \mathbf{0},\ \boldsymbol{\zeta}_i'(0) = \mathbf{P}^{-1}\left(\mathbf{v}_i(0) - \mathbf{C}^T\boldsymbol{\zeta}(0)\right) = \frac{\mathbf{e}_i}{4K_i}.$$

Based on the initial condition for $\boldsymbol{\zeta}_i'(0)$, we have that for s small

$$\boldsymbol{\zeta}_i'(s) = \frac{\mathbf{e}_i}{4K_i} + O(s),$$

which implies that

$$\boldsymbol{\zeta}_i(s) = \frac{s}{4K_i}\mathbf{e}_i + O(s^2). \tag{42}$$

Similarly, we consider the initial value problem which determines $\breve{\boldsymbol{\zeta}}_i(s)$:

$$\mathcal{S}\breve{\boldsymbol{\zeta}}_i = \mathbf{T}_i,\ \breve{\boldsymbol{\zeta}}_i(0) = \mathbf{0},\ \breve{\boldsymbol{\zeta}}_i'(0) = \mathbf{P}^{-1}\left(\breve{\mathbf{v}}_i(0) - \mathbf{C}^T\breve{\boldsymbol{\zeta}}(0)\right) = \mathbf{0}.$$

Unlike the homogeneous case, the initial conditions do not specify the leading-order behavior of $\breve{\boldsymbol{\zeta}}_i(s)$, but they do imply that $\breve{\boldsymbol{\zeta}}_i'(s) = \mathbf{0} + O(s)$, and therefore that $\breve{\boldsymbol{\zeta}}_i(s) = \mathbf{0} + O(s^2)$. Inserting these expressions and the asymptotic relation $\mathbf{C}(s) = \mathbf{C}(0) + O(s)$ into $\mathcal{S}\breve{\boldsymbol{\zeta}}_i$ gives:

$$-\mathbf{P}\breve{\boldsymbol{\zeta}}_i'' + (\mathbf{C}(0) - \mathbf{C}(0)^T)\breve{\boldsymbol{\zeta}}_i' = \mathbf{T}_i + O(s^2),\ \breve{\boldsymbol{\zeta}}_i(0) = \mathbf{0},\ \breve{\boldsymbol{\zeta}}_i'(0) = \mathbf{0}.$$

The asymptotic behavior for $\breve{\boldsymbol{\zeta}}_i$ can then be obtained via a series solution for this IVP (which we produced using the symbolic manipulation package Maple [5]):

$$\breve{\boldsymbol{\zeta}}_1(s) = \begin{bmatrix} O(s^3) \\ \frac{s^2}{4K_2} + O(s^3) \\ O(s^3) \end{bmatrix},\ \breve{\boldsymbol{\zeta}}_2(s) = \begin{bmatrix} -\frac{s^2}{4K_1} + O(s^3) \\ O(s^3) \\ O(s^3) \end{bmatrix},\ \breve{\boldsymbol{\zeta}}_3(s) = \begin{bmatrix} \frac{q_1'(0)s^3}{6K_1} \\ \frac{q_2'(0)s^3}{6K_2} \\ O(s^4) \end{bmatrix}. \tag{43}$$

Given Eqs. (41), (42), and (43), the asymptotic expression for the entire 6×6 constrained stability matrix $\mathbf{M}$ can be computed. The orders (as powers of s) for all 36 entries are known, but the lowest-order coefficients have only been determined for those entries which contribute to the lowest-order term in $\det \mathbf{M}$. Expanding in Maple gives

$$\det \mathbf{M}(s) = \frac{K_2 q_1'(0)^2 + K_1 q_2'(0)^2}{1658880 K_1^3 K_2^3 K_3} s^{14} + O(s^{15}).$$

References

[1] S. S. Antman. *Nonlinear Problems of Elasticity*. Springer-Verlag, New York, 1995.

[2] T. B. Benjamin. The stability of solitary waves. *Proc. R. Soc. Lond. A.*, 328:153–183, 1972.

[3] M. S. Birman and M. Z. Solomjak. *Spectral Theory of Self-Adjoint Operators in a Hilbert Space*. D. Reidel Publishing, 1987.

[4] O. Bolza. *Lectures on the Calculus of Variations*. Chelsea Publishing Company, New York, 1904.

[5] B. Char, K. Geddes, G. Gonnet, B. Leong, M. Monagan, and S. Watt. *Maple V: Library Reference Manual*. Waterloo Maple Software, 1991.

[6] D. J. Dichmann. *Hamiltonian Dynamics of a Spatial Elastica and the Stability of Solitary Waves*. PhD thesis, University of Maryland, College Park, 1994.

[7] E. J. Doedel, H. B. Keller, and J. P. Kernévez. Numerical analysis and control of bifurcation problems, parts I and II. *Int. J. of Bif. and Chaos*, 3, 4:493–520, 745–772, 1991.

[8] G. M. Ewing. *Calculus of Variations with Applications*. Dover Publications, New York, 1969.

[9] I. M. Gelfand and S. V. Fomin. *Calculus of Variations*. Prentice-Hall, Englewood Cliffs, New Jersey, 1963.

[10] J. Gregory and C. Lin. *Constrained Optimization in the Calculus of Variations and Optimal Control Theory*. Van Nostrand Reinhold, New York, 1992.

[11] P. Hagerman. Flexibility of DNA. *Ann. Rewv. Biophys. Chem.*, 17:265–286, 1988.

[12] M. R. Hestenes. *Calculus of Variations and Optimal Control Theory*. Robert E. Krieger Publishing Company, Huntington, New York, 1966.

[13] V. Hutson and J. S. Pym. *Applications of Functional Analysis and Operator Theory*. Academic Press, London, 1980.

[14] T. Kato. *Perturbation Theory for Linear Operators*. Springer-Verlag, Berlin, 1984.

[15] S. Kehrbaum and J. H. Maddocks. Effective bending moduli of elastic rods with high intrinsic twist. *preprint*, 1996.

[16] Y. Li and J. H. Maddocks. On the computation of equilibria of elastic rods, Part I: Integrals, symmetry and a Hamiltonian formulation. *J. Comp. Phys.*, to appear.

[17] J. H. Maddocks. Stability and folds. *Archive for Rational Mechanics and Analysis*, 99(4):301–328, 1987.

[18] R. S. Manning, J. H. Maddocks, and J. D. Kahn. A continuum rod model of sequence-dependent DNA structure. *J. Chem. Phys.*, 105:5626–5646, 1996.

[19] M. Morse. *Introduction to Analysis in the Large*. Institute for Advanced Study, Princeton, New Jersey, 1951.

[20] W. K. Olson. Simulating DNA at low resolution. *Current Opinion in Structural Biology*, 6:242–256, 1996.

[21] M. Reed and B. Simon. *Methods of Modern Mathematical Physics, IV: Analysis of Operators*. Academic Press, San Diego, 1978.

[22] M. Renardy and R. Rogers. *An Introduction to Partial Differential Equations*. Springer-Verlag, New York, 1993.

[23] K. A. Rogers. *Stability Exchange in Parameter Dependent Constrained Variational Principles with Applications to Elastic Rod Models of DNA Minicircles*. PhD thesis, University of Maryland, 1997.

[24] K. A. Rogers and J. H. Maddocks. Stability of elastic rods. *in preparation*, 1996.

[25] H. Sagan. *Introduction to the Calculus of Variations*. Dover Publications, New York, 1969.

[26] T. Schlick. Modeling superhelical DNA: Recent analytical and dynamical approaches. *Current Opinion in Structural Biology*, 5:245–262, 1995.

[27] L. S. Schulman. *Techniques and Applications of Path Integration*. Wiley, New York, 1981.

[28] J. Segercrantz. On the existence of conjugate points for a constrained minimization problem. *J. Comput. Appl. Math.*, 10(3):385–386, 1984.

[29] L. F. Shampine and M. K. Gordon. *Computer Solution of Ordinary Differential Equations: The Initial Value Problem*. W. H. Freeman, San Francisco, 1975.

[30] S. Smith, Y. Cui, and C. Bustamante. Overstretching B-DNA: the elastic response of individual double-stranded and single-stranded DNA molecules. *Science*, 271:795–799, 1996.

[31] T. Vogel. On constrained extrema. *Pacific Journal of Mathematics*, 176, 1996.

[32] A. Weinstein and W. Stenger. *Methods of Intermediate Problems for Eigenvalues: Theory and Ramifications*. Academic Press, New York, 1972.

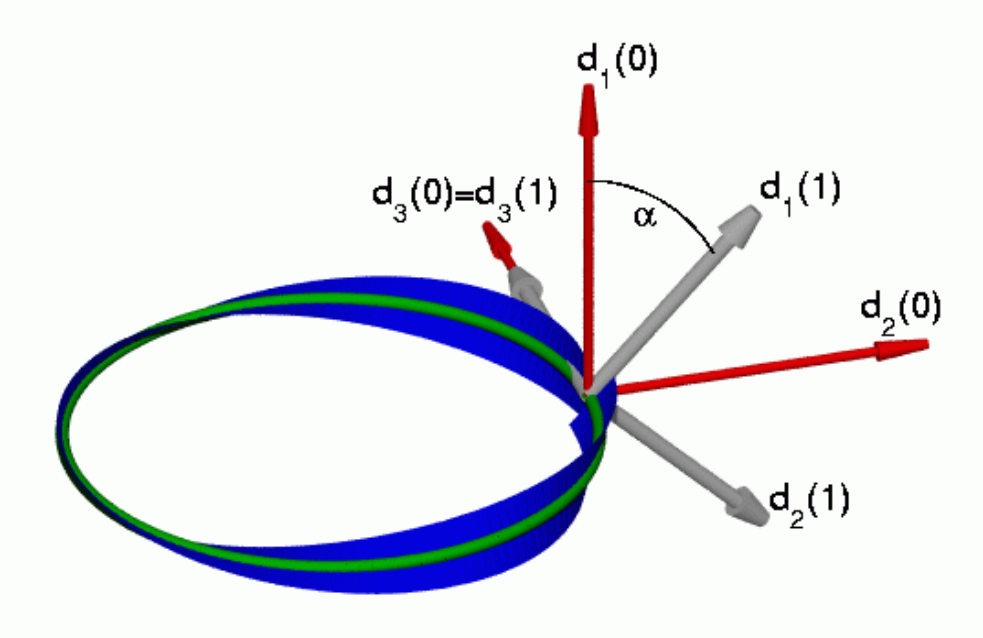

Figure 1: Ring boundary conditions. The centerline $\mathbf{r}$(s) is indicated with a tube, and the normal direction $\mathbf{d}_1(s)$ is visualized as a ribbon. At $s = 0$, the frame is oriented along the standard axes. At $s = 1$, the frame is rotated about $\mathbf{d}_3(0)$ by a prescribed angle α. The $s = 0$ frame is drawn darker and at a larger scale in order to distinguish it from the $s = 1$ frame.

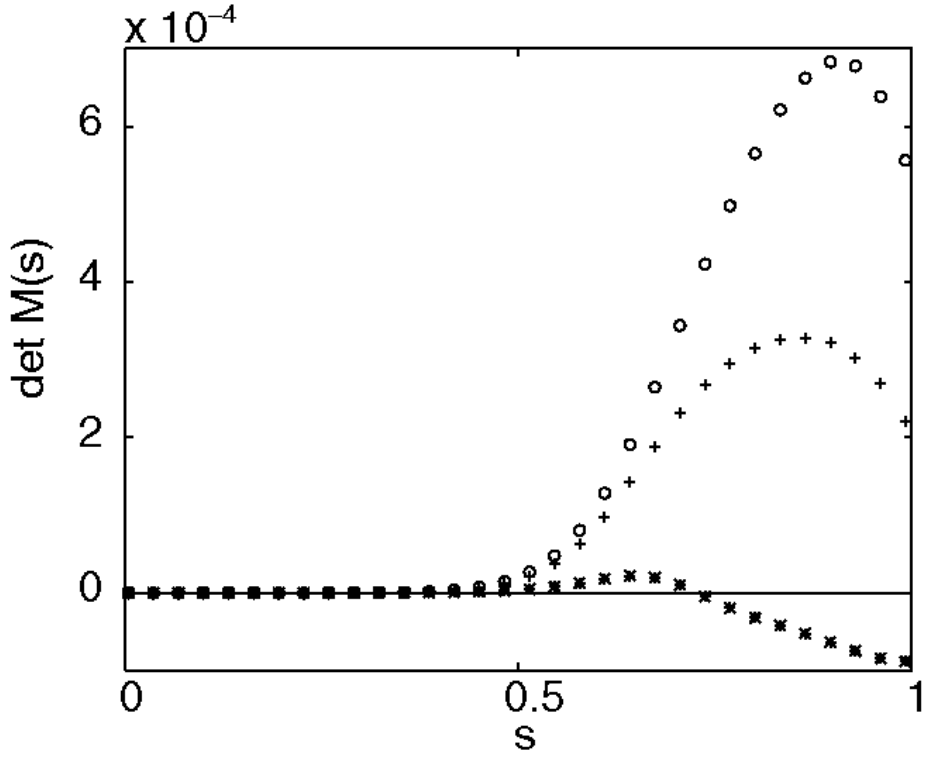

Figure 2: Graphs of the determinant of $\mathbf{M}(s)$ versus arclength for three equilibrium solutions. $\mathbf{M}(0)$ is the zero matrix, and for s close to zero, the determinant is very small but non-zero. Values of $s > 0$ where $\det \mathbf{M} = 0$ are conjugate points. The curves represent three solutions near a fold in the branch of equilibria. The curves of circles ($\circ$) and crosses ($+$) have no conjugate points and thus correspond to stable solutions with isoperimetric index zero. The curve of stars ($*$) has one conjugate point, and thus corresponds to an unstable solution with isoperimetric index one.

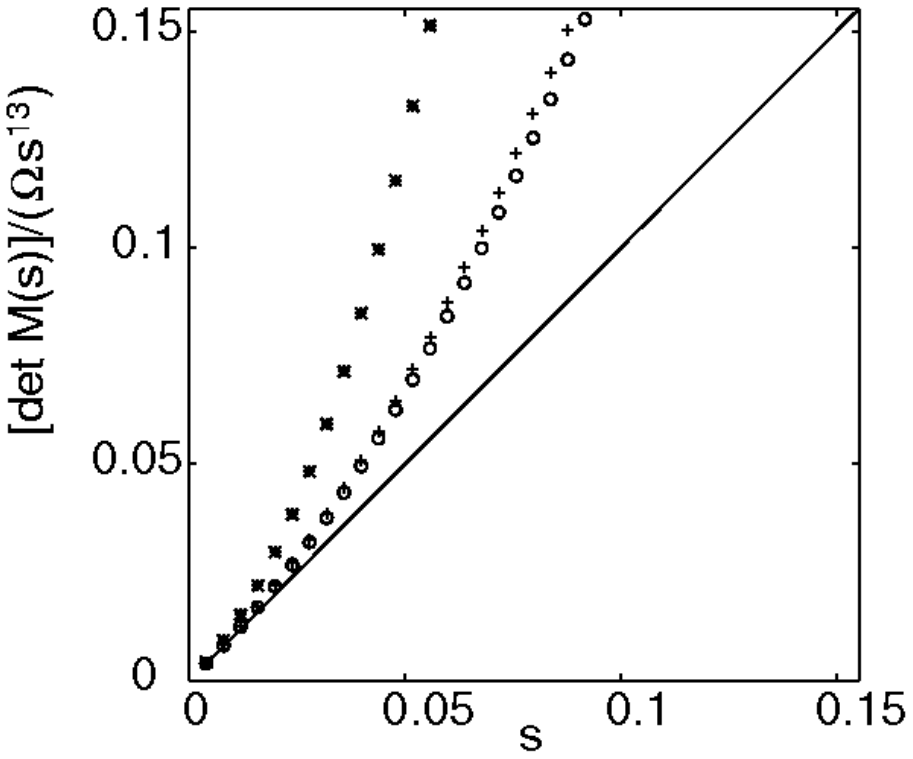

Figure 3: Asymptotic behavior of $\det \mathbf{M}$ near $s = 0$: the three curves from Fig. 2 are depicted, but now for $0 < s < 0.15$ and with the determinant scaled by Ωs^{13} to show that there are no zero crossings near $s = 0$. The data are all tangent to the 45-degree line at $s = 0$, in accordance with the limit (31).

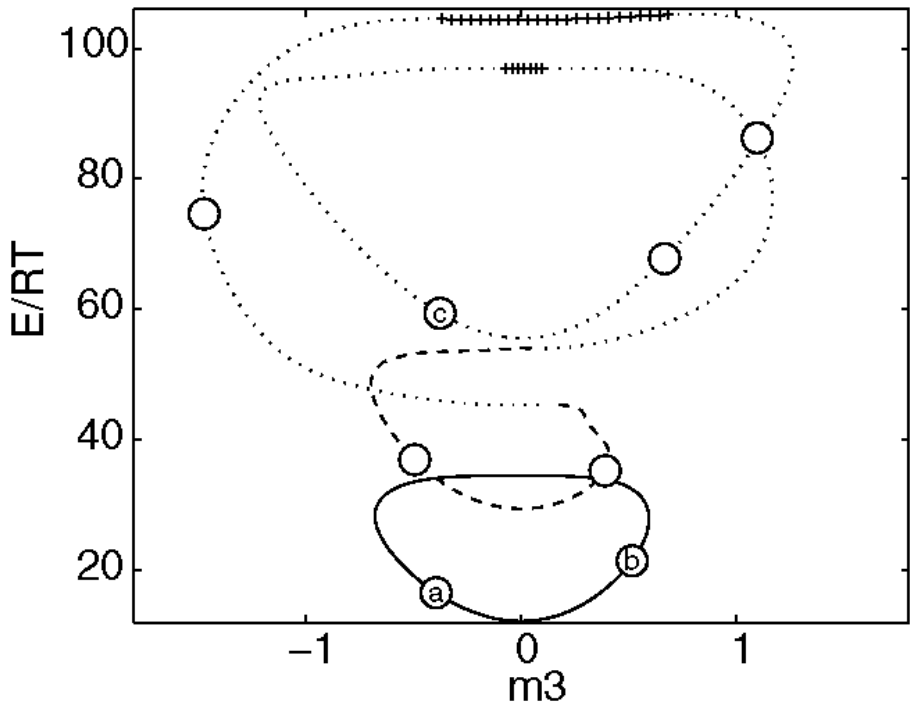

Figure 4: Bifurcation diagram for $\gamma = 1.7$, with the isoperimetric index indicated by line style (solid line= 0, dashed line= 1, dotted line= 2, crosses= 3). In this diagram, branches of equilibria as α varies are represented in a plot of the energy versus the twist moment $m_3(1)$. Cyclized DNA configurations (equilibria with $\alpha = 2n\pi$ and therefore $\mathbf{d}_1(0) = \mathbf{d}_1(1)$) are indicated with circles. The bifurcation diagram shown here contains only the two lowest-energy components of the complete solution set. Each component is a simple closed loop, and there are no bifurcation points (intersections of branches). The crossings seen in the figure are merely a consequence of the particular 2D projection chosen.

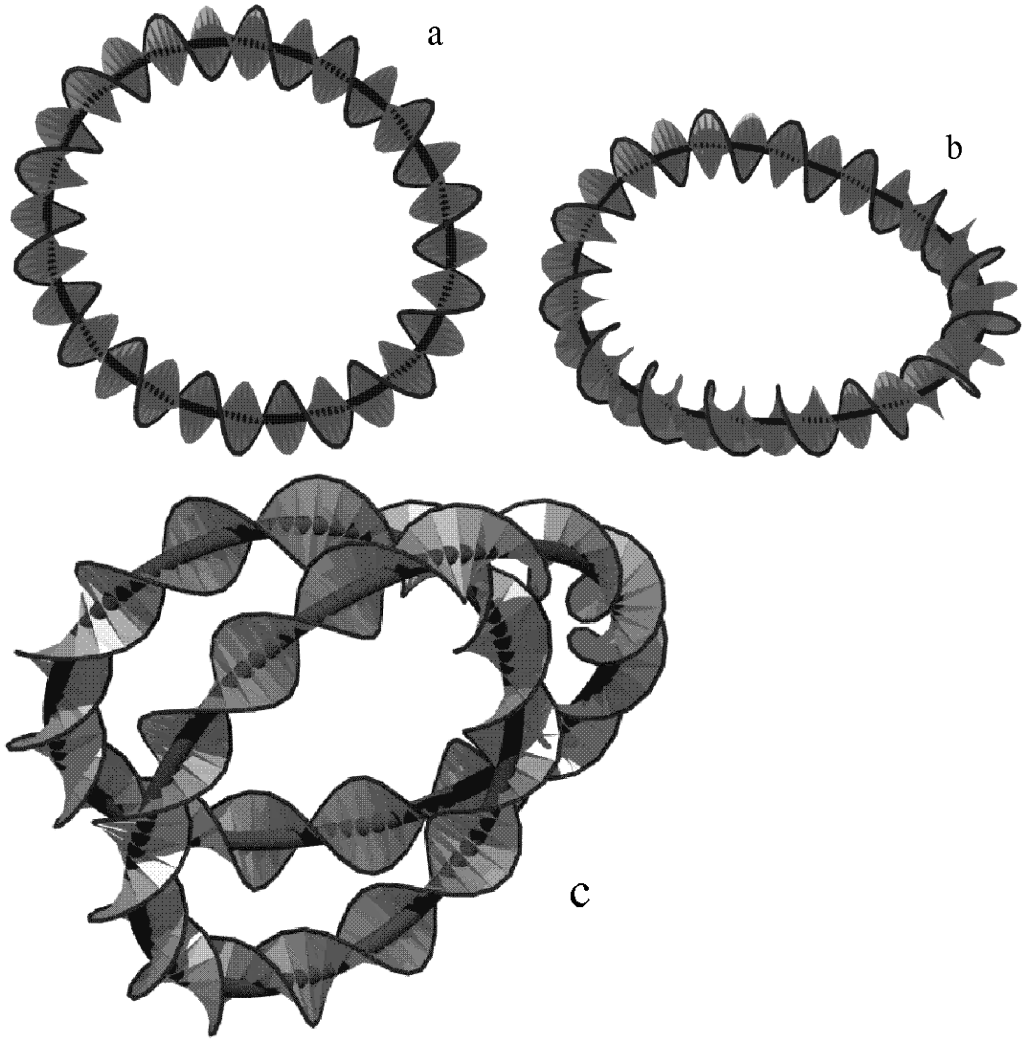

Figure 5: DNA configurations corresponding to the points a, b, and c on the bifurcation diagram in Fig. 4. The centerline is indicated by a tube, and the twist of the double helices by a ribbon. Configurations a and b are stable, with roughly circular centerlines, although configuration a is nearly planar and configuration b is quite non-planar. Configuration c is unstable; its centerline is a perturbation of a double covered circle.

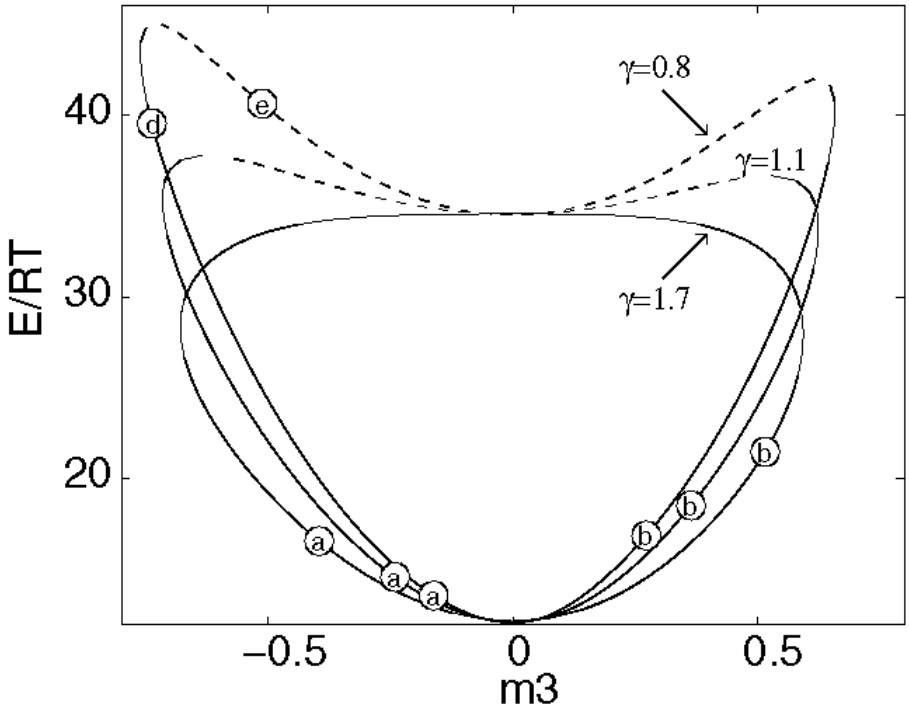

Figure 6: Bifurcation diagrams for DNA cyclization for three values of γ, with isoperimetric index indicated by line style (solid index 0, dashed index 1) ; energy is plotted against twist moment as in Fig. 4. The curve with $\gamma = 1.7$ consists only of stable equilibria. The curves with $\gamma = 1.1$ and $\gamma = 0.8$ have regions of unstable equilibria near the top. Cyclized DNA configurations (equilibria with $\mathbf{d}_1(0) = \mathbf{d}_1(1)$) are indicated with circles. Note that the $\gamma = 0.8$ diagram contains two additional such solutions, labeled d and e. The solution sets shown here are each the lowest-energy component of the complete bifurcation diagram for the labeled value of γ.

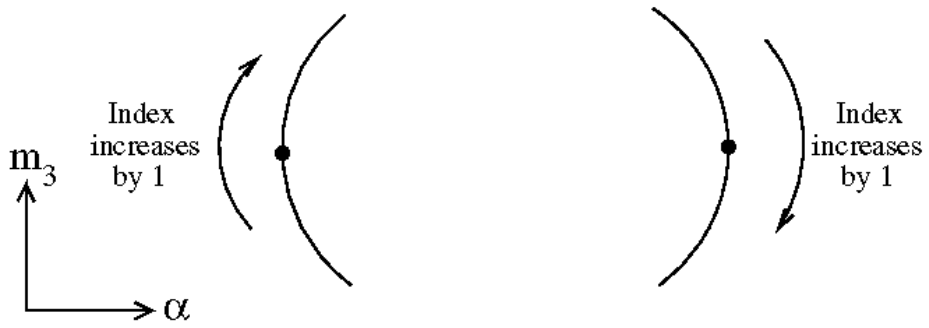

Figure 7: A distinguished bifurcation diagram, in which twist moment m_3 is plotted versus angle α, predicts the direction of the stability exchange at folds (vertical tangents) opening either to the right or to the left.

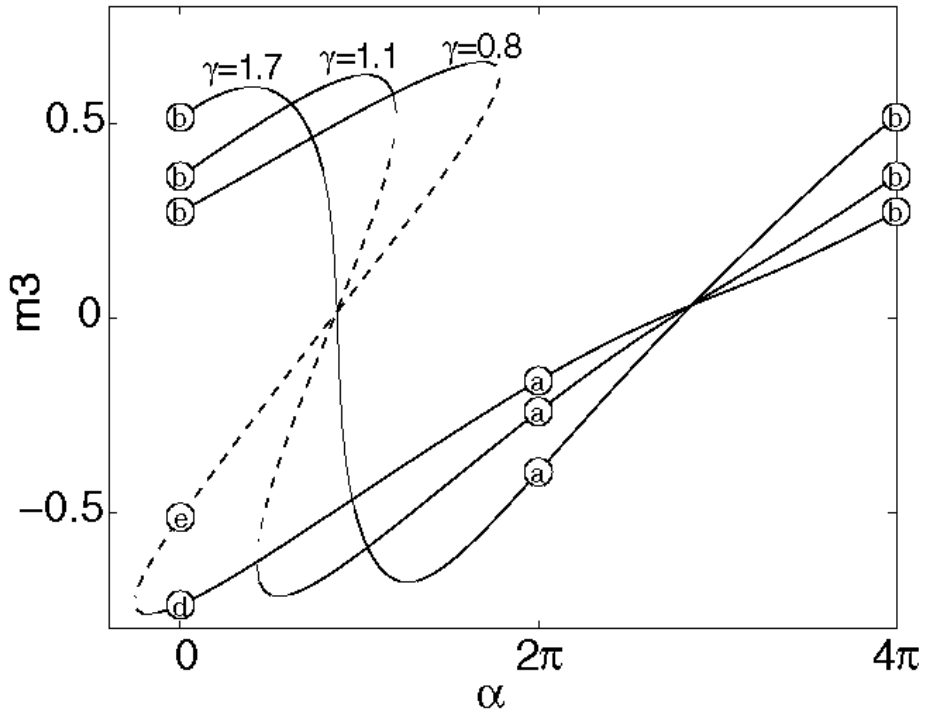

Figure 8: Bifurcation diagrams for DNA cyclization for three values of γ, with isoperimetric index indicated by line style (solid index 0, dashed index 1). The branches of equilibria that are represented are the same ones as in Fig. 6, but now with the twist moment m_3 at $s = 0$ plotted against the angle α. This projection is a distinguished diagram for this problem, so that stability exchanges occur at folds (i.e. at points with vertical tangents) in the specific manner shown in Fig. 7. Cyclized DNA configurations (equilibria with $\mathbf{d}_1(0) = \mathbf{d}_1(1)$) are indicated with circles, which are labeled as in Fig. 6.